NASA TECHNICAL NOTE

NASA TN D-5341

c. 1

NASA TN D-5341

A METHOD OF CHARACTERISTICS FOR STEADY THREE-DIMENSIONAL SUPERSONIC FLOW WITH APPLICATION TO INCLINED BODIES OF REVOLUTION

by John V. Rakich

Ames Research Center
Moffett Field, Calif.

NATIONAL AERONAUTICS AND SPACE ADMINISTRATION • WASHINGTON, D. C. • OCTOBER 1969

1. Report No.	2. Government Accession No.	3. Recipient's Catalog No.
NASA TN D-5341		

4. Title and Subtitle
A METHOD OF CHARACTERISTICS FOR STEADY THREE-DIMENSIONAL SUPERSONIC FLOW WITH APPLICATION TO INCLINED BODIES OF REVOLUTION

5. Report Date
October 1969

6. Performing Organization Code

7. Author(s)
John V. Rakich

8. Performing Organization Report No.
A-3325

9. Performing Organization Name and Address
NASA Ames Research Center
Moffett Field, Calif. 94035

10. Work Unit No.
129-01-03-05-00-21

11. Contract or Grant No.

12. Sponsoring Agency Name and Address
National Aeronautics and Space Administration
Washington, D. C. 20546

13. Type of Report and Period Covered
Technical Note

14. Sponsoring Agency Code

15. Supplementary Notes

16. Abstract

Characteristics theory for three-dimensional compressible flow is reviewed and the compatibility equations are derived in terms of pressure and stream angles as dependent variables. The relative merits of bicharacteristic and reference plane methods are discussed. A reference plane method is described which employs a uniformly spaced finite difference mesh between the body and shock surfaces. Numerical procedures for differentiation and interpolation ensure second-order accuracy in terms of mesh spacing.

Results for the flow around inclined, circular cones, both blunted and pointed, are presented to demonstrate the method described. Predictions of surface and pitot pressures are in good agreement with available experimental results for a 15° sphere-cone at 10° angle of attack. Bluntness effects on shock-layer properties far from the nose are reasonably well predicted.

17. Key Words Suggested by Author
Method of characteristics
Three-dimensional flow
Supersonic flow
Fluid mechanics
Aerodynamics

18. Distribution Statement
Unclassified - Unlimited

19. Security Classif. (of this report)	20. Security Classif. (of this page)	21. No. of Pages	22. Price*
Unclassified	Unclassified	57	$3.00

*For sale by the Clearinghouse for Federal Scientific and Technical Information
Springfield, Virginia 22151

TABLE OF CONTENTS

TABLE OF CONTENTS - Concluded

A METHOD OF CHARACTERISTICS FOR STEADY THREE-DIMENSIONAL SUPERSONIC FLOW WITH APPLICATION TO INCLINED BODIES OF REVOLUTION

By John V. Rakich

Ames Research Center

SUMMARY

Characteristics theory for three-dimensional compressible flow is reviewed and the compatibility equations are derived in terms of pressure and stream angles as dependent variables. The relative merits of bicharacteristic and reference plane methods are discussed. A reference plane method is developed and demonstrated for pointed and blunted bodies at angle of attack.

The fundamental complications arising in a three-dimensional method of characteristics are that: (1) the compatibility equations contain "cross-derivatives" in a noncharacteristic direction; and (2) there is an increased need for interpolation to prevent the computed data surfaces from becoming skewed. These problems are minimized by using a reference plane method with a prescribed and uniform spacing of mesh points. The finite difference mesh employed consists of an equal number of points between the body and shock surfaces in each reference plane. Numerical procedures for differentiation and interpolation ensure second-order accuracy in terms of mesh spacing. Fourier analysis is employed in the circumferential direction and is found to be effective in reducing the number of reference planes and computing times. A typical mesh consists of 7 planes with 15 points in each plane. The unit computation time is about 0.0013 minute per point on an IBM 7094 computer.

Results for the flow around inclined, circular cones, both blunted and pointed, are presented to demonstrate the method described. Predictions of surface and pitot pressures are in good agreement with available experimental results for a 15° sphere-cone at 10° angle of attack. Bluntness effects on shock-layer properties far from the nose are reasonably well predicted.

INTRODUCTION

The method of characteristics has been well known for many years and excellent theoretical developments can be found in numerous texts and reports of which references 1 through 3 give the most complete reviews of multidimensional theory. However, until recent years there have been relatively few practical applications of the methods to three-dimensional flows. This is probably due partly to the large number of operations involved in finite difference calculations in three dimensions, and partly to the extra degree of freedom that results from the existence of characteristic surfaces rather than characteristic lines. High-speed computers have made it technically feasible to perform calculations for three-dimensional steady and unsteady flows and several groups have reported such work. For example, many recent variations on the method of characteristics are reported in references 4 through 10, and a successful use of a noncharacteristic finite difference method is described in reference 11. A number of the proposed characteristics schemes have been described and discussed critically in reference 12.

All the proposed difference schemes for three-dimensional characteristics can be placed in one of two broad categories: (1) reference plane methods (called semi-characteristic methods in ref. 12); and (2) bicharacteristic methods. In reference plane methods the characteristic lines are obtained from the projection of Mach cones and streamlines onto a prescribed plane. In bicharacteristic methods the characteristic lines are the generators of the Mach cone and the actual streamlines. Since, in three dimensions, the equations written along these characteristic lines are partial differential equations, a numerical evaluation of "cross-derivatives" off the characteristic lines is necessary. (In this sense, three-dimensional characteristic methods are similar to noncharacteristic methods for two-dimensional flow.) The problem encountered with most bicharacteristic methods arises from the need to employ a two-dimensional array of data to evaluate the cross-derivatives and to perform the required interpolation in the initial data surface. Furthermore, if a conventional characteristics mesh is used, the distribution of mesh points in the data surfaces tends to become very nonuniform, which causes additional complications. For these reasons one is led to reference plane methods, where a better control can be maintained on the finite difference mesh and where curve fits can be made with respect to a single variable. Reference plane methods have been criticized on the theoretical grounds that the initial data may be outside the domain of dependence of the calculated point. However, problems related to this criticism have not materialized. In fact, the use of such data is precisely what is required by the well-known Courant-Friedrichs-Lewey stability condition.

In the present work, the compatibility equations of characteristic theory are derived for both the bicharacteristic and reference plane methods. Practical difficulties with the bicharacteristic method are discussed and a finite difference scheme based on the reference plane method is proposed. The proposed method abandons the usual characteristic mesh and employs uniformly spaced points along lines lying in equally spaced meridional planes. Numerical interpolation and differentiation are accomplished by means of second-degree polynomials in the radial direction and by Fourier analysis in the circumferential direction.

Preliminary results by the present method were described in reference 13 and compared with calculations by the method of reference 4. Extensive comparisons with experiment were shown in reference 14, establishing the reliability of the numerical methods. In the present report the flow equations and numerical techniques are described in greater detail than was possible in references 13 and 14.

PRINCIPAL SYMBOLS

a	speed of sound
C_1, C_2, C_3	bicharacteristic directions
C_1^*, C_2^*	characteristic directions in meridional planes
C_p	pressure coefficient
C_{p_p}	pitot-pressure coefficient
$\hat{e}_x, \hat{e}_r, \hat{e}_\Phi, \hat{X}_i$	unit vectors along x, r, Φ
h	enthalpy
H	total enthalpy
k	smoothing constant (eq. (84))
$\overline{K}$	coefficient of numerical diffusion term (eq. (84))
M	Mach number
$\hat{N}, \hat{L}, \hat{T}$	shock normal and tangent vectors
p	pressure
R_n	body nose radius
s^*	projection of streamlines on meridional planes
s, n, t	streamline coordinates
u, v, w	velocity components along $\hat{e}_x$, $\hat{e}_r$, $\hat{e}_\Phi$
V	total velocity $\vec{V} = V\hat{s} = V\hat{x}_1$
x	axial distance from blunt nose (body axis)
$\hat{x}_i$	unit vectors along s, n, t
x, r, Φ	cylindrical coordinates
$\hat{y}_i$	unit vectors along characteristic coordinates
$\hat{z}_i$	unit vectors along ξ, η, ζ
α	angle of attack, deg

α_{ij}	transformation matrix (eq. (16))
β	$\sqrt{M^2 - 1}$
γ	specific heat ratio
δ	shock angle in cross plane (eq. (A6))
ε_{ij}	transformation matrix (eq. (A18))
ξ,η,ζ	nonorthogonal shock-layer coordinates (fig. 3)
θ	flow angle from x axis in meridional plane, $\tan^{-1}(v/u)$ (see fig. 1)
λ	angle between $\hat{e}_r$ and $\hat{\eta}$
μ	Mach angle, $\sin^{-1}(1/M)$
μ^*	projection of μ on meridional plane
ν_{ij}	transformation matrix (eq. (A13))
ρ	density
σ	shock angle in meridional plane (eq. (A5))
ϕ	crossflow angle, $\sin^{-1} w/V$ (see fig. 1)
Φ	azimuthal angle, cylindrical coordinates (see fig. 1), deg

Subscripts

A,B	initial and new data lines
b	body
j,τ	indices for radial position of mesh points ($j = 1, 2, \ldots, J - 1, J$) (see fig. 5)
k	index for circumferential position of mesh point ($k = 1, 2, \ldots, L - 1, L$)
n	body nose
s	shock
∞	free-stream condition

Superscripts

i index for axial position of mesh point

ν index denoting variables p, θ, ϕ, ρ for $\nu = 1, 2, 3, 4$

* quantity or component referenced to meridional plane

^ unit vector

$\rightarrow$ general vector

Note: See equation (14) for definition of index notation.

THEORY

Basic Equations of Inviscid Flow

The derivation of the characteristic relations will be carried out in this section starting with the equations for inviscid equilibrium flow written in their intrinsic form with pressure and flow angles as dependent variables. This choice of variables eliminates entropy derivatives from the flow equations, thereby simplifying the analysis. Following the development of reference 15, the combined continuity and momentum equations are written in vector form.

$$\frac{\beta^2}{\rho V^2} \hat{s} \cdot \text{grad } p + \text{div } \hat{s} = 0 \tag{1}$$

$$\frac{1}{\rho V^2} \hat{n} \cdot \text{grad } p + \hat{t} \cdot \text{curl } \hat{s} = 0 \tag{2}$$

$$\frac{1}{\rho V^2} \hat{t} \cdot \text{grad } p - \hat{n} \cdot \text{curl } \hat{s} = 0 \tag{3}$$

where $\hat{s}, \hat{n}, \hat{t}$ are orthogonal unit vectors with $\hat{s}$ tangent to the streamlines. For rotational, inviscid, nonheat-conducting, and nonreacting flow, entropy is conserved along streamlines and this requires

$$\hat{s} \cdot \text{grad } p - a^2 \hat{s} \cdot \text{grad } \rho = 0 \tag{4}$$

Conservation of total enthalpy everywhere gives

$$h + V^2/2 = h_t = \text{constant} \tag{5}$$

Finally, the equation of state may be written as

$$h = h(p,\rho) \tag{6a}$$

or

$$a = a(p,\rho) \tag{6b}$$

In the equations above, if $\hat{n}$ is chosen to lie in meridional planes through the body axis, the unit vectors can be written as follows in terms of flow deflection angles θ and ϕ (see fig. 1).

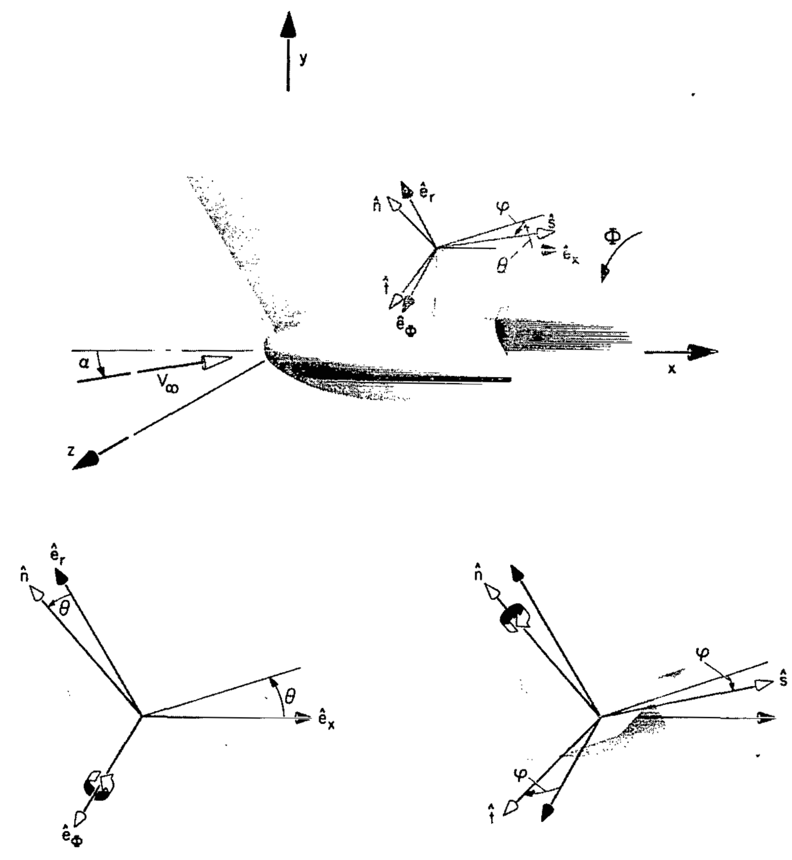

(a) Rotation about $\hat{e}_\phi$. (b) Rotation about $\hat{n}$.

Figure 1.- Cylindrical coordinates.

$$\hat{s} = \cos\phi \cos\theta\, \hat{e}_x + \cos\phi \sin\theta\, \hat{e}_r + \sin\phi\, \hat{e}_\Phi \tag{7}$$

$$\hat{n} = -\sin\theta\, \hat{e}_x + \cos\theta\, \hat{e}_r \tag{8}$$

$$\hat{t} = -\sin\phi \cos\theta\, \hat{e}_x - \sin\phi \sin\theta\, \hat{e}_r + \cos\phi\, \hat{e}_\Phi \tag{9}$$

Using equations (7) through (9) with the standard vector formulas in cylindrical coordinates, one can obtain the following from equations (1) through (4):

$$\frac{\beta^2}{\rho V^2} \frac{\partial p}{\partial s} + \cos\phi \frac{\partial \theta}{\partial n} + \frac{\partial \phi}{\partial t} = - \frac{\cos\phi \sin\theta}{r} \tag{10}$$

$$\frac{1}{\rho V^2} \frac{\partial p}{\partial n} + \cos\phi \frac{\partial \theta}{\partial s} = \frac{\sin^2\phi \cos\theta}{r} \tag{11}$$

$$\frac{1}{\rho V^2} \frac{\partial p}{\partial t} + \frac{\partial \phi}{\partial s} = - \frac{\sin\phi \sin\theta}{r} \tag{12}$$

$$\frac{\partial \rho}{\partial s} = \frac{1}{a^2} \frac{\partial p}{\partial s} \tag{13}$$

Characteristics Theory

Notation.- Characteristics theory is most conveniently developed, especially for the multidimensional case, if one uses index notation. Therefore, the notation and development of Courant and Friedrichs (ref. 1, p. 75) will be followed in this review. Summation convention is used wherein a summation symbol is implied by a repeated index. Thus equations (10) to (12) may be written simply as

$$a^i_{\mu\nu} \frac{\partial u^\nu}{\partial x_i} = f_\mu \tag{14}$$

where the indices refer to:

ν dependent variable (p, θ, ϕ for $\nu = 1, 2, 3$)

i independent variable (s, n, t for $i = 1, 2, 3$)

μ equation (eqs. (10)-(12) for $\mu = 1, 2, 3$)

Coordinate transformation.- Equation (14) can be expressed in terms of new coordinate directions y_j obtained by a rotation of the original coordinates. Thus one can write

$$\hat{x}_i = \alpha_{ij}\hat{y}_j \tag{15}$$

where $\hat{x}_i$ and $\hat{y}_j$ are unit vectors along x_i and y_j, respectively, and the elements of the transformation matrix are the direction cosines defined as follows in terms of the scalar products of $\hat{x}_i$ and $\hat{y}_j$:

$$\alpha_{ij} = \begin{pmatrix} \hat{x}_1 \cdot \hat{y}_1 & \hat{x}_1 \cdot \hat{y}_2 & \hat{x}_1 \cdot \hat{y}_3 \\ \hat{x}_2 \cdot \hat{y}_1 & \hat{x}_2 \cdot \hat{y}_2 & \hat{x}_2 \cdot \hat{y}_3 \\ \hat{x}_3 \cdot \hat{y}_1 & \hat{x}_3 \cdot \hat{y}_2 & \hat{x}_3 \cdot \hat{y}_3 \end{pmatrix} \tag{16}$$

With this transformation, equation (14) becomes

$$b^j_{\mu\nu} \frac{\partial u^\nu}{\partial y_j} = f_\mu \tag{17}$$

where

$$b^j_{\mu\nu} = a^i_{\mu\nu}\alpha_{ij} \tag{18}$$

Characteristic directions and compatibility equations.- If initial data are given for u^ν on the surface $y_1 = 0$, equation (17) can be solved for $\partial u^\nu/\partial y_1$ in order to generate data on an adjoining surface $y_1 = \Delta y_1$. Placing derivatives with respect to y_2 and y_3 on the right side of equation (17), one obtains

$$b^{(1)}_{\mu\nu} \frac{\partial u^\nu}{\partial y_1} = g_\mu \tag{19}$$

where

$$g_\mu = f_\mu - b^k_{\mu\nu} \frac{\partial u^\nu}{\partial y_k} \qquad (k = 2,\ 3)$$

Equation (19) can be considered as a set of algebraic equations for $\partial u^\nu/\partial y_1$, with a solution by Cramer's rule giving

$$\frac{\partial u^\nu}{\partial y_1} = \frac{D^\nu}{\left| b^{(1)}_{\mu\nu} \right|} \tag{20}$$

where $\left| b^{(1)}_{\mu\nu} \right|$ is the determinant of $b^{(1)}_{\mu\nu}$ and D^ν is the determinant obtained by replacing the νth column of $b^{(1)}_{\mu\nu}$ with g_μ.

If $\left| b^{(1)}_{\mu\nu} \right|$ vanishes, then y_1 is normal to a characteristic surface and the flow equations give no information about derivatives in this direction; that is, $\partial u^\nu/\partial y_1$ may be discontinuous. Therefore, the equation of the characteristic surface is given by

$$\left| b^{(1)}_{\mu\nu} \right| = 0 \tag{21}$$

On the other hand, if equation (21) is satisfied, then the numerator of equation (20) must also vanish in order for a solution to exist. Therefore,

$$D^\nu = 0 \qquad (\nu = 1,\ 2,\ 3) \tag{22}$$

gives the so-called compatibility equations. It may be noted from equation (19) that the compatibility relations contain one less dimension than the original differential equations. For the three-dimensional problem the compatibility equations involve derivatives in two directions.

Bicharacteristic Method

The characteristic relations reviewed in the previous section can now be specialized to the problem of equilibrium three-dimensional gas flow. Consider equations (10) through (13) with the supplementary conditions (5) and (6). Note that equation (13) is already in characteristic form since it involves derivatives in one direction; the streamline, s, is a line across which the density gradient, $\partial\rho/\partial n$, may be discontinuous. Therefore, one need only consider equations (10), (11), and (12) for which the i coefficient matrices may be written

$$a_{\mu\nu}^{(i)} = \begin{pmatrix} \delta_{1i} \dfrac{\beta^2}{\rho V^2} & \delta_{2i} \cos \phi & \delta_{3i} \\ \delta_{2i} \dfrac{1}{\rho V^2} & \delta_{1i} \cos \phi & 0 \\ \delta_{3i} \dfrac{1}{\rho V^2} & 0 & \delta_{1i} \end{pmatrix} \tag{23}$$

where δ_{ki} is the Kronecker delta

$$\delta_{ki} = \begin{cases} 0 & k \neq i \\ 1 & k = i \end{cases}$$

The transformed coefficient matrix given by (18) becomes

$$b_{\mu\nu}^{(j)} = \begin{pmatrix} \alpha_{1j} \dfrac{\beta^2}{\rho V^2} & \alpha_{2j} \cos \phi & \alpha_{3j} \\ \alpha_{2j} \dfrac{1}{\rho V^2} & \alpha_{1j} \cos \phi & 0 \\ \alpha_{3j} \dfrac{1}{\rho V^2} & 0 & \alpha_{1j} \end{pmatrix} \tag{24}$$

Characteristic cone.- The characteristic determinant, equation (21), can now be evaluated to give the equation of the characteristic surface in terms of the coefficients of the governing differential equations. Using equation (24) one obtains

$$\left| b_{\mu\nu}^{(1)} \right| = \left(\frac{\alpha_{21}}{\alpha_{11}} \right)^2 + \left(\frac{\alpha_{31}}{\alpha_{11}} \right)^2 - \beta^2 = 0 \tag{25}$$

where $\beta^2 = M^2 - 1$. Now, from equation (16) the terms in equation (25) are recognized as

$$\alpha_{11} = \hat{x}_1 \cdot \hat{y}_1 \qquad \alpha_{21} = \hat{x}_2 \cdot \hat{y}_1 \qquad \alpha_{31} = \hat{x}_3 \cdot \hat{y}_1$$

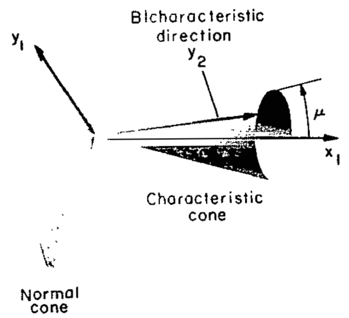

(a) Characteristic cone and bicharacteristics.

Figure 2.- Characteristic coordinates.

which are the components of $\hat{y}_1$ along the $\hat{x}_i$ coordinates. Thus, equation (25) describes a cone around the x_1 or s axis, as indicated in figure 2(a), making the angle $90 - \mu$ with the s direction. This cone is normal to the characteristic cone. The vector $\hat{y}_1$ lies along a generator of the normal cone, and the vanishing determinant (21) means that the derivatives with respect to y_1 may be discontinuous; that is, the differential equations (1), (2), and (3) cannot give any information about derivatives in this direction.

It follows, then, if the y_i coordinates are orthogonal, that $\hat{y}_2$ and $\hat{y}_3$ are tangent to the characteristic cone. If $\hat{y}_2$ is chosen to lie along a generatrix of the cone, then y_2 is called a bicharacteristic direction.

Compatibility equations.- Any one of the three conditions given by equation (22) can be used to obtain the compatibility equations. Consider the case for $\nu = 1$.

$$D_1 = \begin{vmatrix} g_1 & \alpha_{21} \cos \phi & \alpha_{31} \\ g_2 & \alpha_{11} \cos \phi & 0 \\ g_3 & 0 & \alpha_{11} \end{vmatrix} = 0 \tag{26}$$

Expanding (26) one obtains

$$g_1 - (\alpha_{21}/\alpha_{11})g_2 - (\alpha_{31}/\alpha_{11})g_3 = 0 \tag{27}$$

where

$$g_1 = f_1 - \frac{\beta^2}{\rho V^2}\left(\alpha_{12}\frac{\partial p}{\partial y_2} + \alpha_{13}\frac{\partial p}{\partial y_3}\right) - \cos\phi\left(\alpha_{22}\frac{\partial \theta}{\partial y_2} + \alpha_{23}\frac{\partial \theta}{\partial y_3}\right)$$
$$- \left(\alpha_{32}\frac{\partial \phi}{\partial y_2} + \alpha_{33}\frac{\partial \phi}{\partial y_3}\right) \tag{28}$$

$$g_2 = f_2 - \frac{1}{\rho V^2}\left(\alpha_{22}\frac{\partial p}{\partial y_2} + \alpha_{23}\frac{\partial p}{\partial y_3}\right) - \cos\phi\left(\alpha_{12}\frac{\partial \theta}{\partial y_2} + \alpha_{13}\frac{\partial \theta}{\partial y_3}\right) \tag{29}$$

$$g_3 = f_3 - \frac{1}{\rho V^2}\left(\alpha_{32}\frac{\partial p}{\partial y_2} + \alpha_{33}\frac{\partial p}{\partial y_3}\right) - \left(\alpha_{12}\frac{\partial \phi}{\partial y_2} + \alpha_{13}\frac{\partial \phi}{\partial y_3}\right) \tag{30}$$

The bicharacteristic direction y_2 can be arbitrarily chosen to lie along any ray of the characteristic cone. This means that an infinite number of equations can be obtained from (27). However, three equations are sufficient[1] to determine the solution for the three dependent variables p, θ, ϕ.

The bicharacteristics can be chosen so as to simplify the compatibility equations. First it is noted from equation (16), identifying (x_1, x_2, x_3) with (s, n, t), that

$$\alpha_{ij} = \begin{pmatrix} \hat{s}\cdot\hat{y}_1 & \hat{s}\cdot\hat{y}_2 & \hat{s}\cdot\hat{y}_3 \\ \hat{n}\cdot\hat{y}_1 & \hat{n}\cdot\hat{y}_2 & \hat{n}\cdot\hat{y}_3 \\ \hat{t}\cdot\hat{y}_1 & \hat{t}\cdot\hat{y}_2 & \hat{t}\cdot\hat{y}_3 \end{pmatrix}$$

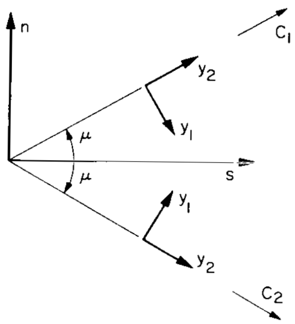

(b) Bicharacteristics in the s-n plane.

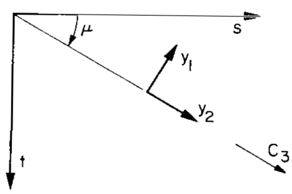

(c) Bicharacteristics in the s-t plane.

Figure 2.- Concluded.

Thus a number of the elements of α_{ij} will be zero if $\hat{y}_2$ is in the s-n plane, and $\hat{y}_3$ lies along the $\hat{t}$ axis. In this case (see fig. 2(b)) there are two possibilities given by

$$\alpha_{ij} = \begin{pmatrix} \sin\mu & \cos\mu & 0 \\ \mp\cos\mu & \pm\sin\mu & 0 \\ 0 & 0 & \pm 1 \end{pmatrix} \tag{31}$$

where the upper sign refers to the left-running characteristic C_1, and the lower sign to the right-running characteristic C_2.

Letting $\hat{y}_2$ lie in the s-t plane so that $\hat{y}_3$ lies along the $\hat{n}$ axis gives

$$\alpha_{ij} = \begin{pmatrix} \sin\mu & \cos\mu & 0 \\ 0 & 0 & -1 \\ -\cos\mu & \sin\mu & 0 \end{pmatrix} \tag{32}$$

where the signs correspond to the bicharacteristic direction C_3 which increases with increasing s and t as shown in figure 2(c).

[1]Redundant schemes which make use of more than three equations are discussed in references 8, 10, 12, and 16.

Substitution of α_{ij} from equations (31) and (32) into equation (27) results in three equations along the bicharacteristics C_1, C_2, and C_3. Using equation (31) for C_1 and C_2, one obtains

$$g_1 \pm \cot \mu \; g_2 = 0$$

where $y_2 = C_1$ for the upper sign and $y_2 = C_2$ for the lower sign. Similarly, one obtains from equation (32) the following equation for the direction C_3:

$$g_1 + \cot \mu \; g_3 = 0$$

Straightforward substitution of the g_i defined in equations (28) to (30) with appropriate elements of α_{ij} from equation (31) or equation (32) yields, with some rearrangement, the following compatibility equations:

$$\frac{\beta}{\rho V^2} \frac{\partial p}{\partial C_1} + \cos \phi \frac{\partial \theta}{\partial C_1} = \left(f_1 + \beta f_2 - \frac{\partial \phi}{\partial t}\right) \sin \mu \tag{33}$$

$$\frac{\beta}{\rho V^2} \frac{\partial p}{\partial C_2} - \cos \phi \frac{\partial \theta}{\partial C_2} = \left(f_1 - \beta f_2 - \frac{\partial \phi}{\partial t}\right) \sin \mu \tag{34}$$

$$\frac{\beta}{\rho V^2} \frac{\partial p}{\partial C_3} + \frac{\partial \phi}{\partial C_3} = \left(f_1 + \beta f_3 - \cos \phi \frac{\partial \theta}{\partial n}\right) \sin \mu \tag{35}$$

where, from the right side of equations (10) through (12),

$$f_1 = -\frac{\cos \phi \sin \theta}{r} , \quad f_2 = \frac{\sin^2 \phi \cos \theta}{r} , \text{ and } \quad f_3 = -\frac{\sin \phi \sin \theta}{r}$$

For two-dimensional flow ($\phi = 0$), equations (33) and (34) reduce to the usual compatibility equations and equation (35) becomes the streamwise momentum equation.

Fundamental complications.- In comparison with axially symmetric flows, equations (33) through (35) have two complicating features which were mentioned earlier. These are (1) the presence of "cross-derivatives" $\partial\phi/\partial t$ and $\partial\theta/\partial n$ on the right side, and (2) the need to perform a two-parameter interpolation for data in the initial data surface. The second problem arises because bicharacteristics through a general mesh point (in a prescribed surface) do not, in general, pass through mesh points in the initial data surface.[2]

Many schemes have been proposed using equations of this form along bicharacteristics (see, e.g., refs. 5-8 and 12). However, the programming of such methods tends to be cumbersome, and the accuracy of evaluating the cross-derivatives is in most cases less than that of the basic calculations. (An exception is the recent work reported in reference 10.) These problems are minimized if characteristics lying in prescribed reference planes are employed. Then the interpolation for initial data and evaluation of cross-derivatives can be reduced to a set of one-parameter curve fits with second-order accuracy. In the next section, the compatibility equations will be derived for characteristic lines which are the projections of bicharacteristics C_1, C_2, C_3 onto reference planes.

Reference Plane Method

In the following development, the flow equations are written in terms of two components lying in predetermined reference planes and a third component directed out of these planes. For most problems encountered in external aerodynamics it is convenient to specify the reference planes as the axial planes, Φ = constant, of a cylindrical coordinate system (see fig. 1). The solution of problems with axial symmetry is determined by calculation along a single plane, but three-dimensional problems require calculation along several planes simultaneously. Characteristic theory is employed to calculate the flow along each plane. To achieve this, the compatibility equations along the projections of the bicharacteristics on the reference planes must be derived. The procedure will be to find the pertinent characteristics and compatibility relations from the intrinsic momentum equations applicable to the reference planes. First, however, it will be necessary to discuss the coordinate mesh which will be used to describe the shock layer.

Finite difference mesh.- The cylindrical coordinate system used to expand the vector relations in equations (1) through (3), and to define the reference planes, is not ideal from the computational standpoint. This stems from the fact that special treatment would be required for bodies with noncircular cross sections and, more importantly, for shock surfaces. One is therefore led to a finite difference mesh which divides the shock layer into a number of annular rings which include both the shock and body surfaces, as shown in figure 3. The resulting mesh points are connected by a nonorthogonal ξ, η, ζ system of coordinates: ξ and η lie in the reference plane with η usually normal to the body surface; ζ is directed out of but not generally normal to the reference plane.

---

[2]Conversely, bicharacteristics through known points on a plane initial data surface will, in general, intersect at points lying in a nonplanar surface. The subsequent data surfaces become increasingly distorted as a computation proceeds away from the initial data plane.

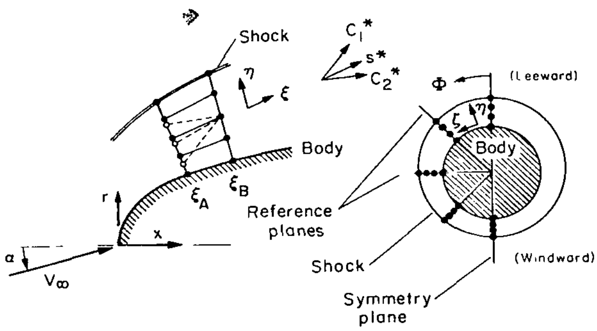

Figure 3.- Nonorthogonal shock-layer coordinates.

A related system is one in which ξ is replaced locally by the projection, s^*, of streamlines onto the reference planes. It is this s^*, η, ζ system which is used to express the intrinsic flow equations (10) through (13) in a form needed for the present reference plane analysis. The unit vectors, $\hat{x}_i = (\hat{s}, \hat{n}, \hat{t})$, in streamline coordinates are related to the new system by direction cosines, ε^*_{ij}, defined by

$$\hat{x}_i = \varepsilon^*_{ij} \hat{z}_j^* \tag{36}$$

where $\hat{z}_j^* = (\hat{s}^*, \hat{\eta}, \hat{\zeta})$.

Written in terms of its components, equation (36) gives

$$\hat{s} = \varepsilon^*_{11} \hat{s}^* + \varepsilon^*_{12} \hat{\eta} + \varepsilon^*_{13} \hat{\zeta} \tag{37}$$

$$\hat{n} = \varepsilon^*_{21} \hat{s}^* + \varepsilon^*_{22} \hat{\eta} + \varepsilon^*_{23} \hat{\zeta} \tag{38}$$

$$\hat{t} = \varepsilon^*_{31} \hat{s}^* + \varepsilon^*_{32} \hat{\eta} + \varepsilon^*_{33} \hat{\zeta} \tag{39}$$

Appendix A describes how ε^*_{ij} is calculated in terms of the body and shock-wave shapes. The detailed expressions for the direction cosines are not needed for the development of this section but it should be noted that, since the shock shape itself is obtained from a solution of the problem (i.e., a direct as opposed to an inverse approach), ε^*_{ij} is not known beforehand for the entire flow. However, in a locally supersonic region, where the shock can be calculated step by step, ε^*_{ij} can always be determined as the calculation proceeds downstream from an initial data line.

Reference plane equations.- Recalling the rules for a directional derivative, equations (37) and (39) yield the following expressions for derivatives in the s and t directions.

$$\frac{\partial}{\partial s} = \varepsilon^*_{11}\frac{\partial}{\partial s^*} + \varepsilon^*_{12}\frac{\partial}{\partial \eta} + \varepsilon^*_{13}\frac{\partial}{\partial \zeta} \tag{40}$$

$$\frac{\partial}{\partial t} = \varepsilon^*_{31}\frac{\partial}{\partial s^*} + \varepsilon^*_{32}\frac{\partial}{\partial \eta} + \varepsilon^*_{33}\frac{\partial}{\partial \zeta} \tag{41}$$

These differentiation rules allow one to write the intrinsic flow equations in terms of the desired planar components. Substituting equations (40) and (41) into equations (10) through (13) and regrouping terms, one obtains

$$\varepsilon^*_{11}\frac{\beta^2}{\rho V^2}\frac{\partial p}{\partial s^*} + \cos\phi\,\frac{\partial\theta}{\partial n} = f_1{}^* \tag{42}$$

$$\frac{1}{\rho V^2}\frac{\partial p}{\partial n} + \varepsilon^*_{11}\cos\phi\,\frac{\partial\theta}{\partial s^*} = f_2{}^* \tag{43}$$

$$\frac{\partial\phi}{\partial s^*} = f_3{}^* \tag{44}$$

$$\frac{\partial\rho}{\partial s^*} = f_4{}^* \tag{45}$$

The left sides of these equations contain derivatives in the reference planes and the remaining terms are all lumped into the $f_i{}^*$, which are given by

$$f_1{}^* = -\frac{\cos\phi\sin\theta}{r} - \left[\frac{\beta^2}{\rho V^2}\left(\varepsilon^*_{12}\frac{\partial p}{\partial\eta} + \varepsilon^*_{13}\frac{\partial p}{\partial\zeta}\right) + \left(\varepsilon^*_{31}\frac{\partial\phi}{\partial s^*} + \varepsilon^*_{32}\frac{\partial\phi}{\partial\eta} + \varepsilon^*_{33}\frac{\partial\phi}{\partial\zeta}\right)\right] \tag{46}$$

$$f_2{}^* = \left[\frac{\sin^2\phi\cos\theta}{r} - \cos\phi\left(\varepsilon^*_{12}\frac{\partial\theta}{\partial\eta} + \varepsilon^*_{13}\frac{\partial\theta}{\partial\zeta}\right)\right] \tag{47}$$

$$f_3{}^* = \frac{1}{\varepsilon^*_{11}}\left[-\frac{\sin\phi\sin\theta}{r} - \frac{1}{\rho V^2}\left(\varepsilon^*_{31}\frac{\partial p}{\partial s^*} + \varepsilon^*_{32}\frac{\partial p}{\partial\eta} + \varepsilon^*_{33}\frac{\partial p}{\partial\zeta}\right) - \left(\varepsilon^*_{12}\frac{\partial\phi}{\partial\eta} + \varepsilon^*_{13}\frac{\partial\phi}{\partial\zeta}\right)\right] \tag{48}$$

$$f_4{}^* = \frac{1}{a^2}\frac{\partial p}{\partial s^*} + \frac{1}{\varepsilon^*_{11}}\left[\varepsilon^*_{12}\left(\frac{1}{a^2}\frac{\partial p}{\partial\eta} - \frac{\partial\rho}{\partial\eta}\right) + \varepsilon^*_{13}\left(\frac{1}{a^2}\frac{\partial p}{\partial\zeta} - \frac{\partial\rho}{\partial\zeta}\right)\right] \tag{49}$$

The $f_i{}^*$ thus expressed contain derivatives along the η and ζ coordinate directions and, as a result, can be easily evaluated with standard one-parameter differentiation routines. It will also be seen, when the finite difference scheme is described, that the derivatives $\partial\phi/\partial s^*$ appearing in $f_i{}^*$ and $\partial p/\partial s^*$ appearing in $f_3{}^*$ and $f_4{}^*$ are easily treated.

It is important to note that, although written in a simplified form, equations (42) through (45) contain no additional approximations beyond those in the original equations. Only the usual assumptions pertaining to viscosity and heat conduction are made. The bracketed [ ] terms in the $f_i{}^*$ all vanish for axially symmetric flows (i.e., for $\phi = 0$), and the equations reduce to the familiar intrinsic equations for zero angle of attack.

Characteristic directions.- Characteristics theory, as outlined in a previous section, can now be applied to equations (42) through (45). It is first observed that equations (44) and (45) are already in the desired characteristic form. These equations give no information about the normal derivative $\partial/\partial n$; therefore, s^* is a characteristic direction for ϕ and ρ. This is in contrast to equations (42) and (43), which can be combined to give derivatives in different directions. Writing the latter in the form of equation (14), one has

$$a^{*i}_{\mu\nu} \frac{\partial u^\nu}{\partial x_i{}^*} = f_\mu{}^* \tag{50}$$

Expressed in terms of new coordinates, $y_i{}^*$, equation (50) becomes (cf. eqs. (17) and (24)):

$$b^{*j}_{\mu\nu} \frac{\partial u^\nu}{\partial y_j{}^*} = f_\mu{}^* \tag{51}$$

where

$$b^{*j}_{\mu\nu} = \begin{pmatrix} \alpha_{1j}\varepsilon^*_{11} \dfrac{\beta^2}{\rho V^2} & \alpha_{2j} \cos\phi \\ \\ \alpha_{2j} \dfrac{1}{\rho V^2} & \alpha_{1j}\varepsilon^*_{11} \cos\phi \end{pmatrix}$$

and where α_{ij} are the elements of the transformation matrix relating x_i and y_j. The characteristic directions for equation (51) are obtained from the determinant

$$\left| b^{*(1)}_{\mu\nu} \right| = 0$$

which yields

$$\left(\frac{\alpha_{21}}{\alpha_{11}}\right)^2 = \varepsilon^{*2}_{11}\beta^2 \tag{52}$$

Writing α_{ij} in terms of a rotation angle as in equation (31), one obtains for this case

$$\alpha_{ij} = \begin{pmatrix} \sin \mu^* & \cos \mu^* \\ \mp\cos \mu^* & \pm\sin \mu^* \end{pmatrix}$$

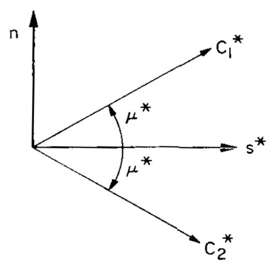

Figure 4.- Characteristic directions for the reference planes.

where μ^* is the angle between the streamline and the characteristics in the reference plane as shown in figure 4. Equation (52) shows that μ^* is related to the Mach angle according to

$$\cot \mu^* = \varepsilon^*_{11} \cot \mu \tag{53}$$

Compatibility equations.- The compatibility equations applicable to the directions C_1^* and C_2^* can be obtained in the way previously described for the bicharacteristics. For the present case, one has in place of equation (27)

$$g_1^* - \frac{\alpha_{21}}{\alpha_{11}} g_2^* = 0 \tag{54}$$

where

$$g_1^* = f_1^* - b^{*(2)}_{11} \frac{\partial u^{(1)}}{\partial y_2} - b^{*(2)}_{12} \frac{\partial u^{(2)}}{\partial y_2}$$

and

$$g_2^* = f_2^* - b^{*(2)}_{21} \frac{\partial u^{(1)}}{\partial y_2} - b^{*(2)}_{22} \frac{\partial u^{(2)}}{\partial y_2}$$

Algebraic details are straightforward and need not be repeated. The resulting compatibility equations are:

$$\frac{\beta}{\rho V^2}\frac{\partial p}{\partial C_1{}^*} + \cos\phi\,\frac{\partial\theta}{\partial C_1{}^*} = (f_1{}^* + \beta f_2{}^*)\sin\mu^* \tag{55}$$

$$\frac{\beta}{\rho V^2}\frac{\partial p}{\partial C_2{}^*} - \cos\phi\,\frac{\partial\theta}{\partial C_2{}^*} = (f_1{}^* - \beta f_2{}^*)\sin\mu^* \tag{56}$$

Equations (55) and (56), together with equations (44) and (45), are the final set of differential equations programmed for numerical calculations. They are supplemented by the energy equation (eq. (5))

$$h + V^2/2 = H$$

and the equations of state ((6a) and (6b))

$$h = h(p,\rho)$$

and

$$a = a(p,\rho)$$

Details of the numerical methods used in the computer program are described in the next section.

NUMERICAL METHODS

The general theory of characteristics was developed in the previous section, where it was shown that the three-dimensional problem can be reduced to an equivalent two-dimensional form. A numerical solution of the problem can then be accomplished in the usual way by numerically evaluating derivatives in one direction in order to calculate a step forward in the second direction. The problem is analogous to the numerical solution of two-dimensional hyperbolic equations by noncharacteristics methods.

Therefore, in formulating a practical method for calculating three-dimensional flow, the numerical differentiation process is of primary importance. If the differentiation is to be performed efficiently and accurately (i.e., at least second order in a typical mesh dimension), the mesh points should be constrained to lie along simple coordinate lines. Secondly, the boundary calculations are simplified if the coordinates lie on the shock and body surfaces. These considerations suggest the shock-layer-oriented, nonorthogonal coordinates shown in figure 3. The resulting computational procedure is simplified significantly compared with previously proposed three-dimensional characteristics methods (see, e.g., ref. 12).

Presented next are the difference equations, computational logic, and numerical differentiation procedures developed on the basis of this nonorthogonal (ξ, η, ζ) mesh. The problem may be stated as follows:

> Given data on an initial $\eta - \zeta$ surface at ξ_o where the flow is locally supersonic, it is required to generate, by means of the flow equations and boundary conditions, new data on the adjacent $\eta - \zeta$ surface at $\xi_o + \Delta\xi$.

Finite Difference Equations

Figure 5 shows the mesh point arrangement for a typical reference plane Φ_k. Identify with superscripts (i-1) and (i) the initial data line at ξ_A and new data line at ξ_B. Let the subscripts j and k denote the radial and circumferential positions of the mesh points. However, the subscript k will be omitted for brevity in writing the difference equations.

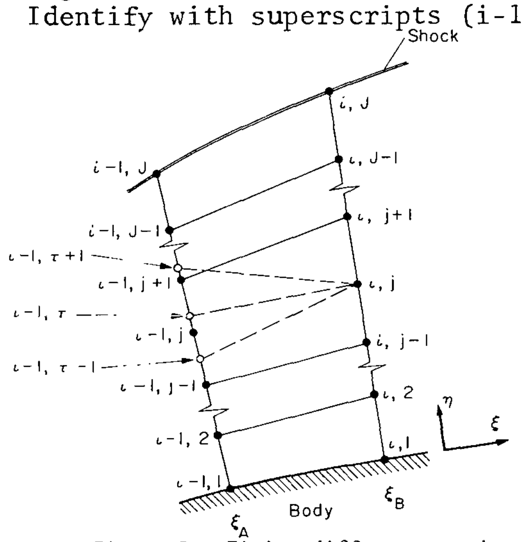

Figure 5.- Finite difference mesh.

The method adopted[3] to calculate conditions at a typical mesh point i,j on ξ_B makes use of interpolated data at the points of intersection on ξ_A of the characteristics through point i,j. A three-point Lagrange interpolation is employed to determine the necessary data from known conditions at neighboring mesh points.

Three intersections are required for each field point on ξ_B. To identify these points the convention is adopted whereby the subscript τ represents the intersection with ξ_A of the streamline projection s^* through point i,j, and the subscripts $\tau-1$ and $\tau+1$ represent intersections of characteristics C_1^* and C_2^*, respectively (see fig. 5).

With this convention the compatibility equations (55) and (56) can be written in the following finite difference form:

$$A_1\left(p_j^{\,i} - p_{\tau-1}^{\,i-1}\right) + B_1\left(\theta_j^{\,i} - \theta_{\tau-1}^{\,i-1}\right) = F_1\ \Delta C_1^* \tag{57}$$

$$A_2\left(p_j^{\,i} - p_{\tau+1}^{\,i-1}\right) - B_2\left(\theta_j^{\,i} - \theta_{\tau+1}^{\,i-1}\right) = F_2\ \Delta C_2^* \tag{58}$$

---

[3]This method is called the Hartree method (ref. 17) and also the inverse method (ref. 12); it was used by Katskova and Chushkin (ref. 9).

Equations (44) and (45) are similarly written as

$$\phi_j^{\ i} - \phi_\tau^{\ i-1} = F_3 \ \Delta s^* \tag{59}$$

and

$$\rho_j^{\ i} - \rho_\tau^{\ i-1} = F_4 \ \Delta s^* \tag{60}$$

The system of equations is completed by the energy and state equations, (5) and (6). They apply to all of the field points - that is, for the index j running from 2 up to $J-1$. For the body point, $j=1$, equation (57) is replaced by the equation of the body,

$$r_1^{\ i} = f(x_1^{\ i}, \Phi_k)$$

which permits the calculation of $\theta_1^{\ i}$ by means of equations derived in appendix C. It is shown there that

$$\tan \theta_1^{\ i} = \frac{1}{1 - a^2}\left(\frac{\partial r_1^{\ i}}{\partial x} + a\sqrt{b - a^2}\right) \tag{61a}$$

where

$$a = \tan \phi\left(\frac{1}{r_1^{\ i}} \frac{\partial r_1^{\ i}}{\partial \Phi}\right) \quad \text{and} \quad b = 1 + \left(\frac{\partial r_1^{\ i}}{\partial x}\right)^2$$

For bodies of revolution equation (61a) reduces to

$$\theta_1^{\ i} = \tan^{-1} \frac{\partial r_1^{\ i}}{\partial x} \tag{61b}$$

At the shock, $j = J$, equations (58), (59), and (60) are replaced by the oblique shock equations. The jump conditions for a general three-dimensional shock surface are developed in appendix B and can be written in the following functional form for fixed free-stream conditions:

$$(u^\nu)_j^{\ i} = G^\nu\left(\sigma^i; \delta_k, \Phi_k, \alpha\right) \tag{62}$$

where u^ν represents p, θ, ϕ, ρ for $\nu = 1, 2, 3, 4$. Here σ and δ are the shock-wave angles in the planes Φ = constant and x = constant, respectively, and α is the angle of attack. Equation (62) depends directly on the unknown shock angle σ^i, and indirectly on the parameters δ_k, Φ_k, and α. The shock angle δ_k is determined by numerical differentiation of shock coordinates as described in appendix A. The four equations obtained from (62) for $\nu = 1$ through 4, together with equation (57), are sufficient to determine the shock angle σ^i.

Computational Procedure

Local iteration.- The difference equations are solved by a standard Euler predictor-corrector method in which the coefficients are treated as constants locally and equal to their average value over the step. An initial guess, say $(u^\nu)_j^i = (u^\nu)_j^{i-1}$, is used to start an iterative procedure by which corrected values of $(u^\nu)_j^i$ are calculated using coefficients evaluated with the previous predictions. The iteration is continued until the pressure repeats to a specified accuracy. For typical mesh points three correctors reduce the relative error to less than 1×10^{-5}. It is shown in standard texts that the iterated result has a truncation error of the order of the step size cubed.

In this method the coefficients A_μ, B_μ, and F_μ in equations (57) through (60) are averaged along the characteristic direction appropriate to each equation. For example, the coefficient F_1 in difference equation (57) represents the average of the right side of differential equation (55), taken along the characteristic $C_1{}^*$, and is written as

$$F_1 = 1/2[(f_1{}^* + \beta f_2{}^*)]_j^i + 1/2[(f_1{}^* + \beta f_2{}^*)]_{\tau-1}^{i-1} \tag{63}$$

in the present notation. Similarly, averages are evaluated using data at point $\tau+1$ for equation (58) and at point τ for equations (59) and (60).

Global iteration.- The set of equations (57) through (60) are solved successively on L reference planes, Φ_k $(k = 1, 2, \ldots, L)$. The difference equations governing the flow along various reference planes are coupled by cross-derivatives which are included in the functions F_μ appearing on the right side of each equation and by the shock angle δ_k appearing in equation (62). In order to solve these equations in an explicit manner, it is therefore necessary first to approximate F_μ and δ_k with derivatives evaluated on ξ_A. Then, using calculated values on all of the L planes to evaluate cross-derivatives on ξ_B, one obtains the next approximation to F_μ and δ_k and the entire process can be repeated. This is referred to as a global iteration, in contrast to the point-by-point iteration employed in the local solution of the difference equations.

Since computing times are generally large in three-dimensional problems (see next section), test cases were run to determine the need for global iteration. Table I shows that excellent results are obtained without iteration, that is, using derivatives evaluated on ξ_A. It is therefore expected that this iteration would not be required in most problems.

Step Size

Since the mesh points are not constrained to follow characteristic lines with the present method, the size of a forward step, $\Delta\xi = \xi_B - \xi_A$, can be arbitrary to some extent. The only limitation is that, in order to have a stable numerical process, the step should not exceed a certain maximum determined by the region of influence of the initial data. This stability condition will make $\Delta\xi$ depend on the radial step $\Delta\eta$, smaller radial steps requiring smaller forward steps. The lateral step $\Delta\zeta$ does not affect the stability directly, although it does, of course, affect the accuracy. The effect of step size on accuracy is discussed after the following paragraphs on stability condition.

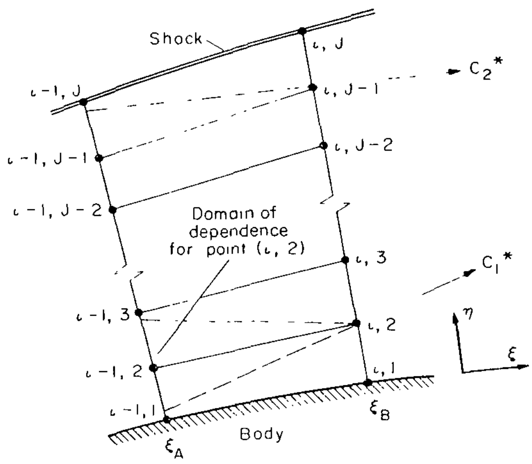

Figure 6.- Step size limitation.

Stability condition.- Although the analysis of numerical stability has not been performed for the general nonlinear equations, the stability criterion for linear hyperbolic equations (see, e.g., ref. 17) is apparently sufficient for the nonlinear equations. This is the well-known C-F-L (Courant, Friedrichs, Lewey) condition which essentially states that the domain of dependence of the calculated point must be included in the initial data. This means that the characteristic C_1* through point (i,2) in figure 6 must pass through or above point (i-1,1). Similarly, the characteristic C_2* through point (i,J-1) must fall through or below point (i-1,J).

Strictly followed, the C-F-L condition would require testing every shock and body point to determine the maximum allowable step size, $\Delta\xi_m$, which would insure stability. However, experience indicates that the condition is not overly restrictive in the sense that steps slightly larger than $\Delta\xi_m$ do not usually cause a violent instability. Therefore, it is adequate to test only at the body and, for bodies with circular cross section, on the windward side where $\Delta\xi_m$ is likely to be smallest, due to the low Mach number. The step size is then taken slightly less than the maximum; a value of $\Delta\xi = 0.8\ \Delta\xi_m$ works well in most problems.

Accuracy and computing time.- The accuracy of a numerical computation is usually estimated by comparing results obtained with various mesh spacings.

Since the exact solution is usually unknown, one can only compare with the results of the finest mesh and observe how the error decreases. If the truncation errors are second order in terms of the mesh size, then halving the mesh size should reduce the error by one-quarter.

To test the accuracy of the present method, calculations were performed from $x/R_n = 2$ to $x/R_n = 3$, using 3, 5, and 7 planes and 5, 10, and 15 points along each plane. In each case the same starting conditions were used at $x/R_n = 2$. The results of this study are shown in table II. Table II(a) presents the shock angles and the surface pressure on the $\Phi = 90°$ plane at $x/R_n = 3$. These results show that the method is of second-order accuracy. Also, it should be noted that the results with $k = 5$ and 7 agree very well for J fixed (moving horizontally in the table). The good accuracy with only a few planes is attributed to the use of trigonometric analysis for the cross-derivatives.

The computing time naturally increases as the mesh is refined; this is illustrated in table II(b), which lists the total number of points computed, the total execute time, and the time per point in minutes. The calculation was performed on an IBM 7094 Model 1 in FORTRAN IV (version 13 IBJOB processor). A unit time of about 0.13×10^{-2} min per point was obtained with the finest mesh. The unit time increases as the number of points decreases, probably because of fixed input/output times. The actual and unit times are almost doubled when one global iteration is made at each station.

Numerical Differentiation

Discussed next is the problem of evaluating cross-derivatives appearing in the equations. Partial derivatives in three directions appear in the functions f_i^* defined by equations (46) through (49). They are of the form $\partial/\partial s^*$, $\partial/\partial\eta$, and $\partial/\partial\zeta$, in the stream, radial, and circumferential directions. Special treatment is given to the circumferential derivative, following the discussion of the first two.

Streamwise and radial derivatives.- These derivatives are taken together since they are both evaluated by the standard polynomial approach. The main idea is to employ a differentiation formula consistent with the accuracy of the basic calculation.

For the streamwise derivative the approximation

$$\frac{\partial u^\nu}{\partial s^*} = \frac{(u^\nu)_j^i - (u^\nu)_\tau^{i-1}}{\Delta s^*} \tag{64}$$

is clearly equivalent to the form of the difference equations employed. Equation (64) represents the derivative of u^ν at the midpoint of the interval, $\Delta s^*/2$, with an error of the order Δs^{*2}. This derivative is evaluated at each step in the local iteration process previously described.

Because of the equally spaced coordinate mesh presently employed, the radial derivative is similarly determined to the same accuracy by the central difference

$$\frac{\partial u^{\nu}}{\partial \eta} = \frac{(u^{\nu})^{i}_{j+1} - (u^{\nu})^{i}_{j-1}}{2\ \Delta\eta} \tag{65}$$

Equation (65) approximates the derivative at point (i,j) with an error of order $\Delta\eta^2$. The average radial derivative at the midpoint (i+1/2,j) between ξ_A and ξ_B can be obtained by means of the global iteration procedure previously described.

Standard end-point formulas of equivalent accuracy are used at the body and shock where central differences are not possible. These need not be written out, as they can be found in many books (e.g., ref. 18).

Circumferential derivatives.- In the aerodynamics of bodies it is well known, from linearized and perturbation theories as well as from experiment, that the solution of most problems can be represented by a trigonometric series in the meridional angle Φ. When information such as this is available it should be possible, by choice of an appropriate functional form, to improve a numerical process. For example, with data known to have a nearly cosine variation, it is clear that fewer sample points are required to approximate the data with a cosine series than with a polynomial. A Fourier-series approximation is therefore used to evaluate derivatives with respect to ζ. Symmetry conditions, which usually arise at $\Phi = 0$ and $\Phi = \pi$, are easily satisfied in this way. This technique makes it possible to calculate with fewer reference planes, thereby increasing the computational efficiency (see ref. 13).

For the present application it is necessary to determine Fourier approximations for pressure p, flow angle θ, crossflow angle ϕ, and density ρ from their values on L planes Φ_k (k = 1, 2, . . . , L) with $\Phi_1 = 0$ and $\Phi_L = \pi$. Symmetry conditions for three variables (represented by u_k^{ν} (ν = 1, 2, 4)) are satisfied by a cosine series of the form

$$u_k^{\nu} = \sum_{n=0}^{L-1} a_n^{\nu} \cos n\ \Phi_k \qquad (\nu = 1,\ 2,\ 4) \tag{66}$$

For the crossflow angle (ν = 3), which is zero at $\Phi = 0$ and $\Phi = \pi$, a sine series

$$\phi_k = \sum_{n=1}^{L-1} b_n \sin n\ \Phi_k \tag{67}$$

is necessary.

When equally spaced meridional planes $\Phi_k = \pi(k - 1)/(L - 1)$, $(k = 1, 2, \ldots, L)$ are used, the calculation of the Fourier coefficients is particularly simple because the usual orthogonality conditions are exactly satisfied by a finite sum (see, e.g., ref. 18 or 19). In this case the coefficients are given by

$$a_n^{\nu} = \frac{2}{L - 1}\left[\frac{\left(u_1^{\nu} + u_L^{\nu} \cos n\pi\right)}{2} + \sum_{k=2}^{L-1} u_k^{\nu} \cos n\,\Phi_k\right] \quad (n = 0, 1, \ldots, L - 1) \qquad (68)$$

and

$$b_n = \frac{2}{L - 1}\sum_{k=2}^{L-1} \phi_k \sin n\,\Phi_k \qquad (n = 1, 2, \ldots, L - 1) \qquad (69)$$

Derivatives with respect to the angle Φ are obtained by differentiating the Fourier series, equations (66) and (67), to give

$$\frac{du_k^{\nu}}{d\Phi} = \sum_{n=1}^{L-1} -na_n^{\nu} \sin n\,\Phi_k \qquad (70)$$

and

$$\frac{d\phi_k}{d\Phi} = \sum_{n=1}^{L-1} nb_n \cos n\,\Phi_k \qquad (71)$$

The desired derivatives in terms of distance along the ζ direction are obtained from equations (70) and (71) according to

$$\frac{\partial}{\partial\zeta} = \frac{1}{g_{\zeta}}\left(\frac{d}{d\Phi}\right)_{\text{on } \zeta} \qquad (72)$$

where it is understood that the derivative on the right side of (72) is evaluated using data on the ζ coordinate. The scale factor g_{ζ} relates the distance along ζ corresponding to an incremental change in Φ,

$$g_{\zeta} = \frac{d\zeta}{d\Phi}$$

and can be written in terms of the direction cosines developed in appendix A. From these coordinate relations one has

$$r(d\Phi/d\zeta) = \hat{e}_\Phi \cdot \hat{\zeta} \equiv \overline{\nu}_{33}$$

and therefore,

$$g_\zeta = (r/\overline{\nu}_{33}) \tag{73}$$

Starting Data

The method of characteristics, being a method for initial value problems, requires starting data which are usually obtained from boundary conditions or from an initial solution obtained by other methods. For present applications two types of starting conditions are of particular interest. These are (1) the spherically blunted body with the sonic line located on the spherical nose, and (2) pointed bodies which can be approximated by a cone in some small region near the tip.

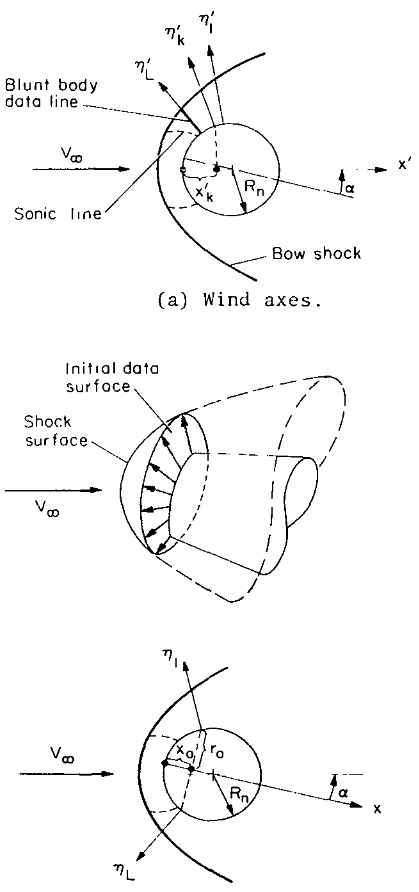

(a) Wind axes.

(b) Body axes.

Figure 7.- Starting data for a spherical nose.

Sphere.- Since a sphere does not have a preferred orientation, the flow remains symmetric around the wind axis for any angle of attack. Therefore, axisymmetric blunt-body solutions obtained, for example, by the inverse method of reference 20 can be used to provide initial conditions. It is necessary, however, to generate these axisymmetric starting data on an initial η-ζ surface which is defined in a body axis system; the data will not be symmetric with respect to the body axis.

The characteristics program is set up to generate body axis data from wind axis data obtained from a blunt-body solution. Given these wind axis data on one body normal (see fig. 7(a)) where the flow is supersonic, say $M > 1.05$, the characteristics calculation is performed in a wind axis system and for $\alpha = 0$ to the position x_k', locating the body normals η_k'. (Primes denote wind axes.) This is illustrated in figure 7(a). Since the flow is axisymmetric in terms of wind axes, the normals η_k' may be placed at an arbitrary circumferential position. The values of x_k' are chosen so that the normals η_k' match the ring of normals η_k emanating from the sphere at (x_o,r_o) in terms of body axes (fig. 7(b)). They are related to the meridional angle Φ_k and the angle of attack α by

$$x_k' = R_n + (x_o - R_n)\cos\alpha - r_o \sin\alpha \cos\Phi_k \tag{74}$$

where R_n is the radius of the spherical nose.

Scalar data derived in this way on the body normals η_k ($k = 1, 2, \ldots, L$) are ready for use in the general three-dimensional calculation. However, the flow angles, θ and ϕ, must be recalculated in terms of body axes by means of the transformation relationships for velocity components. By the definition of θ and ϕ (fig. 1).

$$\theta = \sin^{-1} \frac{v}{V \cos \phi} \tag{75}$$

$$\phi = \sin^{-1} \frac{w}{V} \tag{76}$$

The magnitude of the velocity is unchanged by the coordinate rotation, so that

$$V = V' \tag{77}$$

From reference 15, the velocity components v, w can be expressed as follows in terms of wind axis components:

$$v = (u' \sin \alpha + v' \cos \alpha \cos \Phi')\cos \Phi + v' \sin \Phi' \sin \Phi \tag{78}$$

$$w = v' \sin \Phi' \cos \Phi - (u' \sin \alpha + v' \cos \alpha \cos \Phi')\sin \Phi \tag{79}$$

where Φ' is obtained from

$$\cot \Phi \sin \Phi' - \cos \alpha \cos \Phi' - \frac{(x' - R_n)}{r'} \sin \alpha = 0 \tag{80}$$

Equations (75) through (80) determine θ and ϕ, relative to body-axis coordinates, from u' and v' calculated in the wind-axis system.

Cone.- Conical solutions are defined as those which are independent of ξ - that is, all derivatives with respect to ξ vanish. Conical flows can be obtained in two ways: (1) by solving the boundary value problem for the reduced equations with $\partial/\partial\xi = 0$ (see, e.g., ref. 21), or (2) by the asymptotic solution of three-dimensional initial value problem with a conical body (see ref. 11 or 22). The latter approach is presently taken since it fits the general computation scheme with little change.

Approximate initial data for a cone are specified and the calculation downstream is carried on until the conical flow condition is met to a specified accuracy.[4] This approach has the disadvantage of being generally more time-consuming than the boundary value method, but it avoids many difficulties inherent in boundary value problems. The situation is quite similar to the calculation of the supersonic blunt-body problem by an asymptotic

---

[4]It is clear physically that the conical condition must be obtained far downstream from the approximate starting condition.

unsteady calculation. Approximate starting conditions are obtained either from the perturbation solution for cones at small angle of attack (ref. 23) or from a previous three-dimensional solution for a different Mach number or cone angle.

Two modifications to the general computational procedure are required to obtain the correct conical flow solutions for circular cones. First, it was found necessary to account for the Ferri vortical layer (ref. 24) by setting the entropy at all body points, except at the leeward plane of symmetry, equal to the entropy at the windward shock point. The entropy at the leeward body station, which is a singular point, must equal the entropy at the leeward shock point.[5] Thus the following conditions apply to circular cones:

$$\left.\begin{aligned} S_{1,k} &= S_{J,L} \qquad (k = 2, 3, \ldots, L) \\ &\text{and} \\ S_{1,1} &= S_{J,1} \end{aligned}\right\} \tag{81}$$

Secondly, as a result of the entropy singularity at the leeward body point, the circumferential density derivative there is also singular. Therefore, data from the singular point must be excluded in the numerical differentiation for $\partial\rho/\partial\zeta$.

Smoothing

Under certain conditions where the density or crossflow angle develop large radial gradients, the numerical calculation for these quantities appears to be unstable. This situation can arise in the region of the vortical layer on pointed cones and in the so-called entropy layer over blunted cones. A stabilizing difference scheme similar to that known as the Lax, or Lax-Wendroff method (refs. 26 and 27) is therefore used in these cases.

Equations (59) and (60) are modified for this purpose according to the following difference approximation:

$$(u^\nu)_j^i - (u^\nu)_j^{i-1} = \left\{ F_\nu + \frac{k\ \Delta\eta^3}{2\eta_J\ \Delta\xi} \frac{\left[(u^\nu)_{j-1}^{i-1} - 2(u^\nu)_j^{i-1} + (u^\nu)_{j+1}^{i-1}\right]}{\Delta\eta^2} \right\} \Delta s^* \tag{82}$$

where $\nu = 3$ or 4 represents ϕ or ρ, respectively. The second term in the bracket is proportional to the second derivative of u^ν, so that the

[5]Additional singular points arise in more general conical flows (see, e.g., ref. 24 or ref. 25).

difference equation (82) approximates the differential equation[6]

$$\frac{\partial u^{\nu}}{\partial s^*} = F_{\nu} + \overline{K}\,\frac{\partial^2 u^{\nu}}{\partial \eta^2} \tag{83}$$

where

$$\overline{K} = \frac{k\ \Delta\eta^3}{2\eta_J\ \Delta\xi} \tag{84}$$

and η_J is the value of η at the shock $\eta_J = (J - 1)\Delta\eta$.

The additional term in equation (83) represents a diffusion process and is the stabilizing term in the type of difference scheme given by equation (82). The arbitrary constant k in equation (84) is included to allow control of the diffusion term. If $k = 0$, equation (83) reduces to equation (59) or equation (60). For $k = \eta_J/\Delta\eta$, equation (83) is essentially the same as the Lax scheme (ref. 26).

It is known (this is demonstrated below) that the Lax difference scheme provides too much diffusion; therefore, it is desirable to choose k between 0 and $\eta_J/\Delta\eta$ in order to provide numerical stability without undue loss of accuracy. In most applications k has been set equal to 1, and this condition is presently termed a second-order Lax smoothing because in this case

$$\overline{K} = \frac{\Delta\eta}{2\eta_J\ \Delta\xi}\,\Delta\eta^2 = 0(\Delta\eta^2) \tag{85a}$$

Thus, the second-order difference scheme approaches the differential equation like $\Delta\eta^2$ as the mesh is refined, whereas the Lax method approaches linearly in $\Delta\eta$. For large Mach numbers, an order-of-magnitude analysis reveals that

$$\overline{K} = 0\left(\frac{1}{M_J{}^2}\right) \tag{85b}$$

which gives $\overline{K}$ a value of about 1/1000 for a typical mesh.

---

[6]This argument is not strictly rigorous, as pointed out in reference 27, if the dissipative term is of the same order as the truncation error of the other terms. Nevertheless, the analogy is qualitatively correct, especially when the step size is not small. Also, when the integration is carried over large distances the truncation error might tend to be random, while the dissipative term is always additive.

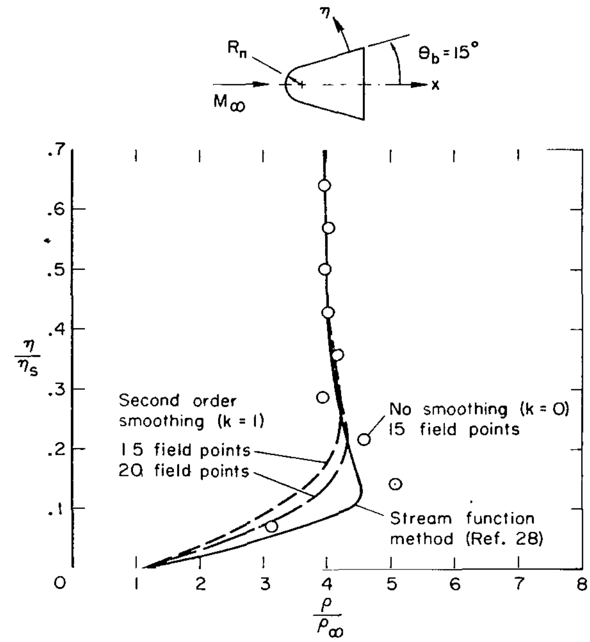

Figure 8.- Effect of smoothing on density distribution at $x/R_n = 40$; 15° sphere-cone, $M_\infty = 10$, $\alpha = 0$.

The effect of this difference approximation is illustrated in figure 8 for a 15° sphere-cone at zero angle of attack. The figure shows the density distribution in the shock layer at a station 40 nose radii downstream from the stagnation point.

Calculations by the present method are compared with the method of reference 28 which accurately determines the density distribution in axisymmetric flow by the use of a stream function. Present results with second-order smoothing are shown in figure 8 by the broken lines for 15 and 20 mesh points. It is seen that these curves differ from the more exact result only where the second derivative, $\partial^2\rho/\partial\eta^2$, is large, and that the error decreases as the mesh is refined. Results obtained without smoothing and with 15 mesh points are shown by the symbols. The calculations appear to be unstable without smoothing.

It is emphasized that the need for smoothing arises only when the computational mesh is coarse relative to the details of the flow field. Experience indicates that the smoothing can be eliminated if the mesh is refined sufficiently. This, however, is not practical in three-dimensional problems where computation time and computer storage limitations are important factors. Therefore the proposed smoothing scheme provides a means for obtaining meaningful results with a relatively coarse mesh of points.

Discontinuous derivatives.- The possibility of discontinuities in supersonic flows presents a severe test for a numerical calculation. With the present numerical method, characteristic lines are not followed and some smearing of the discontinuities will occur because of the interpolation for data on

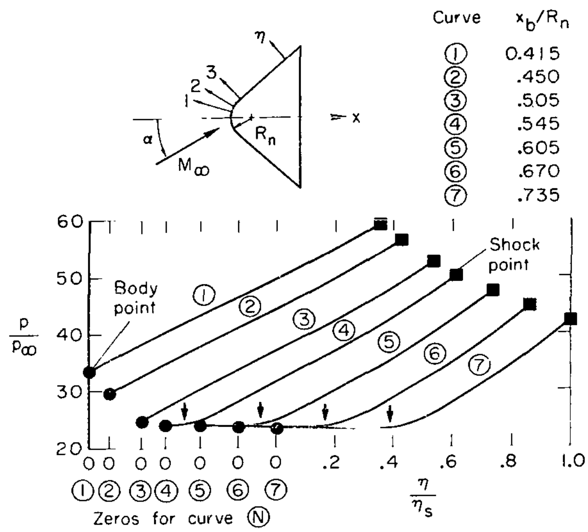

(a) Leeward plane, $\Phi = 0°$.

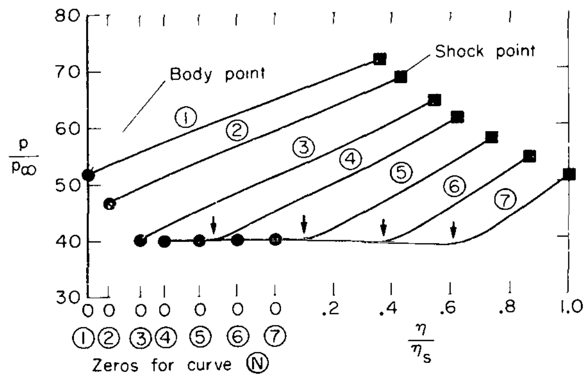

(b) Windward plane, $\Phi = 180°$.

Figure 9.- Pressure distribution on surface normals, η; 30° sphere-cone, $M_\infty = 10$, $\alpha = 5°$.

the initial data line. This problem was therefore investigated and it was found that the proposed method does provide an accurate resolution of known flow details obtained with a standard method of characteristics for axisymmetric flow (ref. 29).

Discontinuous derivatives arise primarily on the body surface at points where the surface curvature is not analytic. As an example, figure 9 shows a map of the pressure in the vicinity of the sphere-cone juncture for a blunted cone at 5° angle of attack. Each line represents the pressure variation along a body normal, η, between the body and the shock wave. The origin for each line is displaced in proportion to the x coordinate of the body point so that the circular symbols represent the actual surface-pressure distribution. The surface pressure decreases uniformly on the spherical nose until the sphere-cone juncture is reached, at $x_b = 0.5$, where the pressure gradient, $\partial p/\partial s$, changes abruptly. The discontinuity from that point moves out into the flow field along a Mach wave. (The approximate position of the wave is indicated by the arrows.) The pressure is nearly constant behind the wave and varies according to the blunt-nose flow ahead of the wave. The curves theoretically should have a discontinuous slope there. As seen in the figure, the curves are only slightly rounded by the quadratic interpolation presently employed.

RESULTS AND DISCUSSION

Many numerical solutions have been obtained with the described method of characteristics, and these results compare favorably with other published works (see, ref. 13). Presented in this section are the details of a typical calculation for a 15° sphere-cone at 10° angle of attack and a Mach number of 10. This is considered to be sufficiently nonlinear to provide a good test of the theory. The dominant three-dimensional features of the flow are illustrated and compared with predictions of perturbation methods for small angles of attack. Bluntness effects are illustrated by comparison with a pointed cone solution, which is described first.

Pointed Cone

The solution for a pointed 15° cone at a Mach number of 10.6 and 10° angle of attack is presented in table III. Listed for each plane, Φ = constant, are the shock angles, σ and δ. Below the shock angles are tabulated the x,r coordinates of each mesh point running from the shock to the body and the corresponding flow variables at those points, as labeled. The quantity M^* is the component of Mach number defined by the Mach angle μ^* in equation (53). Remaining variables are defined in the list of symbols.

This conical solution was obtained with a coordinate mesh consisting of 9 meridional planes and with 11 points on each plane. Second-order smoothing was used on the density ρ and the crossflow angle ϕ (smooth constant $k = 1$). Initial data for the present case were obtained from a previous solution at $M = 7$ which agreed with the tabulated results of reference 11. The free-stream Mach number was changed from 7 to 10 and the computation was carried downstream until the flow relaxed to the new conical solution. This was accomplished in a number of stages, with each stage consisting of a computation from $x = 0.8$ to 1.0, using the output of the previous stage as initial data.

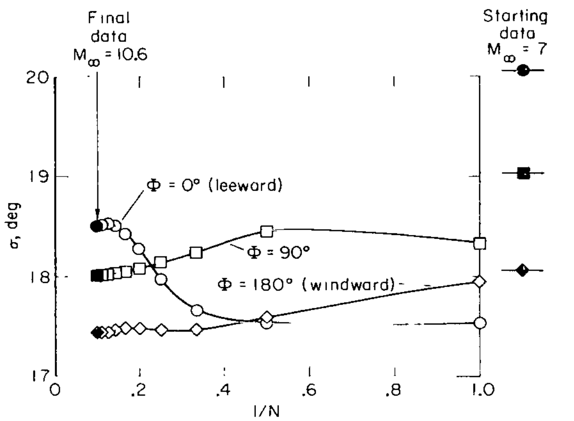

Figure 10.- Relaxation of conical solution after N stages of calculation from $x = 0.8$ to $x = 1.0$; 15° cone, $M_\infty = 10.6$, $\alpha = 10°$.

The accuracy of the solution is indicated by figure 10 which shows the shock angle in three meridional planes as a function of the reciprocal of the number of stages. It is seen that the approximate starting conditions cause the shock angles to change abruptly in the first stage with a slow decay to a limiting value as 1/N tends to zero. Conditions on the lee side are slowest to approach a limit. The shock angle at $\Phi = 0$ repeated to an accuracy of $\Delta\sigma/\sigma = 0.45\times10^{-3}$ in the last stage of calculation and repeated to an accuracy of 1×10^{-5} during the last step of the tenth stage.

The main features of this conical flow will be illustrated in conjunction with the blunted cone results described next.

Spherically Blunted Cone

The calculation for a spherically blunted cone with a 15° semivertex angle in air ($\gamma = 1.4$) at $M_\infty = 10$ used 7 meridional planes with 15 points in each plane. Second-order smoothing, $k = 1$, was employed for the 10° angle-of-attack solution when $x/R_n > 10$; no smoothing was necessary for the other solutions presented.

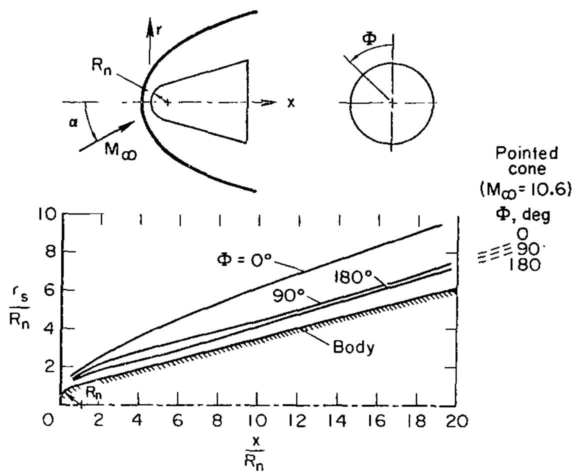

Figure 11.- Shock trace on meridional planes; 15° sphere-cone, M_∞ = 10, α = 10°.

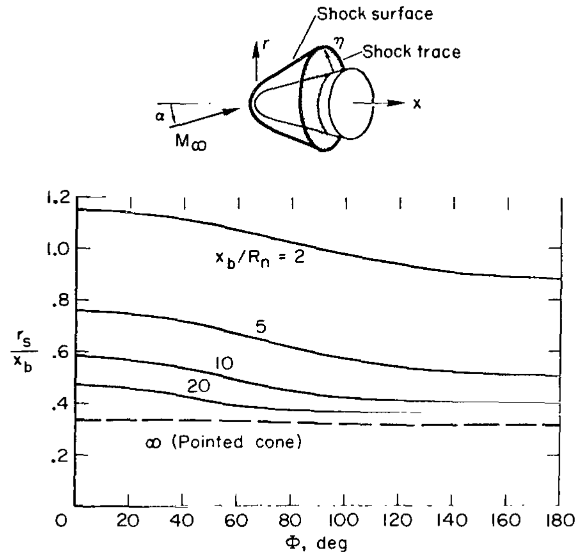

Figure 12.- Shock trace on body-normal surfaces; 15° sphere-cone, M_∞ = 10, α = 10°.

The shock profiles in three meridional planes are shown in figure 11 for a cone length of 20 nose radii. Also shown on the figure are the pointed-cone shock positions which the blunt-cone shock must approach as x/R_n gets large. The small difference in the Mach number of the two solutions of 10 to 10.6 does not significantly affect the comparison. It is observed that the shock quickly approaches the pointed-cone shock for $\Phi = 90°$ and $\Phi = 180°$, while it does not appear to approach the pointed limit on the lee side, $\Phi = 0°$. This is further illustrated in figure 12, which shows the circumferential shock shape for several axial stations. The slow decay on the lee side is evidenced by the hump in the profile near $\Phi = 0$. Note that the x coordinate is not constant on the shock traces shown, because the shock radial position is measured at its intersection with a cone normal to the body surface (see sketch in fig. 12).

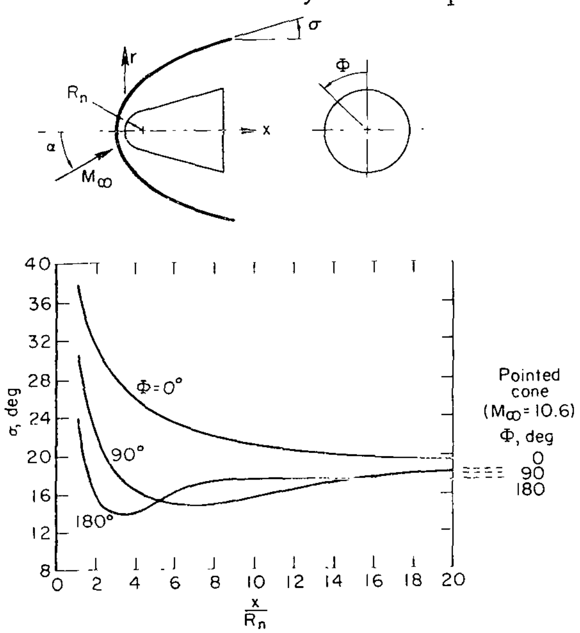

Figure 13.- Shock angles in meridional planes; 15° sphere-cone, M_∞ = 10, α = 10°.

The axial distribution of shock angle is shown in figure 13. On the windward plane, $\Phi = 180°$, the angle reaches a minimum value of 13.744° at $x/R_n = 3.89$. On the leeward plane the angle has not reached a minimum by $x/R_n = 20$ and is still well above the pointed-cone value at that point.

In a three-dimensional flow the streamlines generally flow across the meridional planes as a result of the asymmetrical pressure distribution. This crossflow is described in terms of the angle ϕ which is related to the

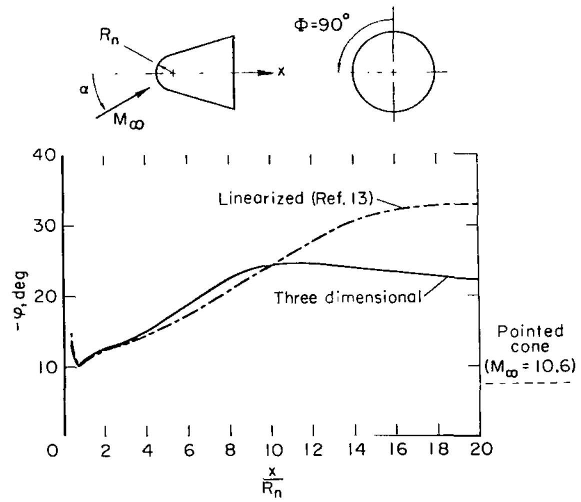

Figure 14.- Axial distribution of surface crossflow angle; 15° sphere-cone, M_∞ = 10, α = 10°, Φ = 90°.

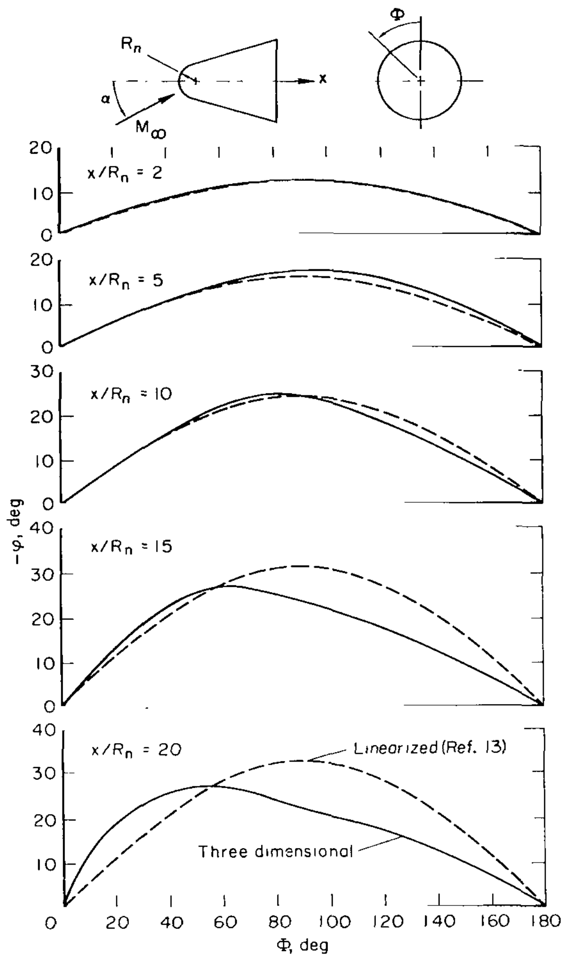

Figure 15.- Circumferential distribution of surface crossflow angle; 15° sphere-cone, M_∞ = 10, α = 10°.

familiar crossflow velocity according to $\phi = \sin^{-1}$ (w/V). Figure 14 shows the axial distribution of crossflow angle along the side meridian Φ = 90°. The crossflow angle is a minimum at the sphere-cone juncture and then rises to a maximum value about 2.4 times the angle of attack. Thus, the surface upwash for blunted bodies can be greater than the maximum value of 2α given by slender-body theory, which applies to pointed bodies at low supersonic speeds. It is interesting also to compare the result of the linearized characteristics method (ref. 15) which is in good agreement near the nose. Agreement extends to about x/R_n = 10, where the linear method starts to break down.

The reason for the breakdown is evident in figure 15 which shows the circumferential variation of ϕ for α = 10° at various axial stations. Near the nose the variation is nearly sinusoidal, as assumed in the linearized method. However, the exact three-dimensional calculations show a large deviation from the sinusoidal variation beyond x/R_n = 10.

Figure 16 shows the variation of crossflow angle normal to the body. The curve for x_b/R_n = 20 approaches the pointed-cone solution near the shock, η/η_s = 1, but deviates by a large amount near the body. This is due to the low density of the flow in the entropy layer which is generated near the body surface by the blunt nose. The flow in this region has less momentum that that away from the surface, and is therefore turned more by the circumferential pressure gradient. The situation is analogous to boundary-layer

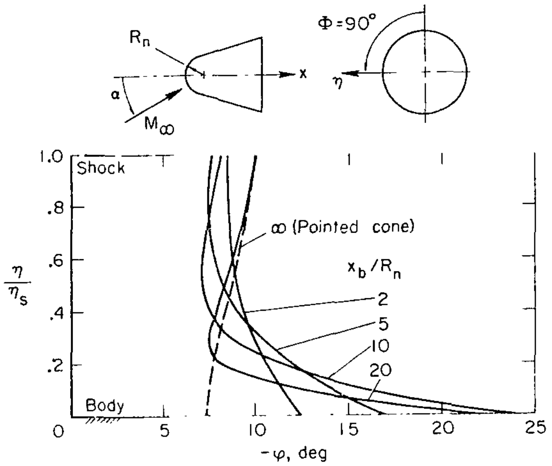

Figure 16.- Radial distribution of crossflow angle; 15° sphere-cone, M_∞ = 10, α = 10°, Φ = 90°.

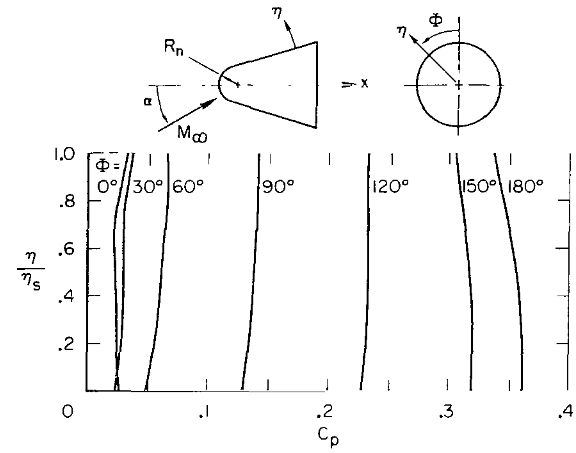

Figure 17.- Radial distribution of static pressure; x_B/R_n = 16.7, 15° sphere-cone, M_∞ = 10, α = 10°.

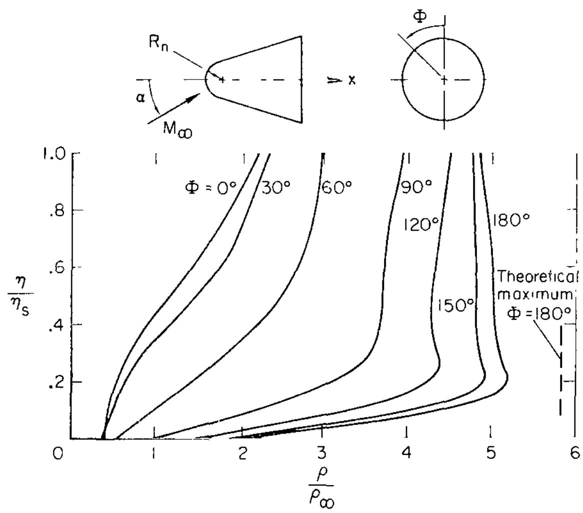

Figure 18.- Radial distribution of density; x_B/R_n = 16.7; 15° sphere-cone, M_∞ = 10, α = 10°.

flow over an inclined body.[7] Therefore, because of the entropy layer, the blunt-cone crossflow does not approach the pointed-cone distribution uniformly.

The entropy layer is characterized by a nearly constant pressure, as is shown in figure 17. On the other hand, the density varies strongly on the windward side of the body as may be seen in figure 18 for x_b/R_n = 16.7. The thickness of the entropy layer may be taken as the distance to the point where the density has a local maximum. This entropy layer is similar to that found in axisymmetric flow except that it develops faster (i.e., closer to the nose) on the windward side and more slowly on the lee side of the body. Smoothing, which was used to stabilize the calculation, causes the peak in density to be rounded off. A theoretical maximum for Φ = 180° can be calculated by using the entropy corresponding to the minimum shock angle and by making use of the fact that the pressure is nearly constant. The theoretical maximum is about 15 percent higher than the calculated value. It is estimated that the smoothing had negligible effect on the density and crossflow angle for η/η_s greater than about 0.3 (see fig. 8).

[7]Comparison is made in reference 14 between inviscid and experimental (viscous) surface streamlines.

Comparison With Experiment

Detailed experimental surveys of the flow field around blunted cones have been previously reported by Cleary (refs. 30 and 31). Experimental results from reference 30 are used to compare with the present theoretical results in order to confirm the validity of the proposed numerical methods. More complete comparisons between theory and experiment can be found in references 31 and 14, for both air and helium flows.

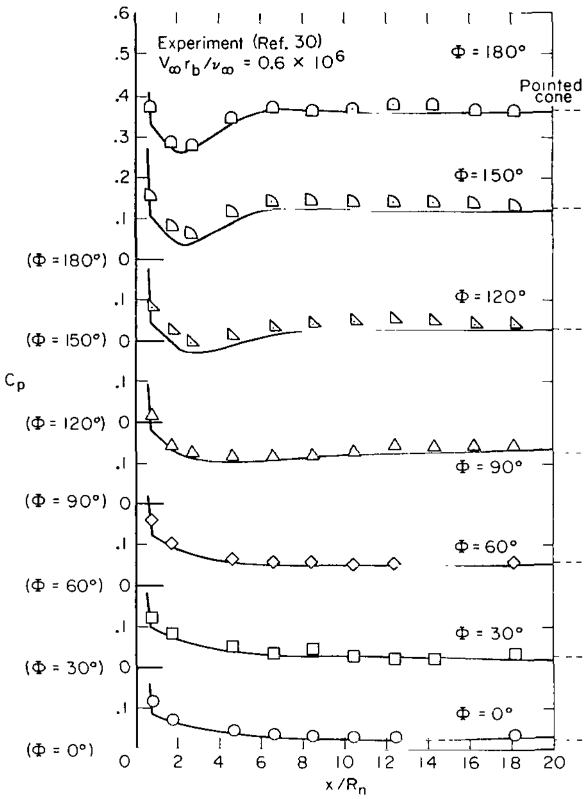

Figure 19.- Surface pressure distribution; 15° sphere-cone, $M_\infty = 10$, $\alpha = 10°$.

Figure 19 presents the surface pressure distribution along each of the 7 meridional planes along which the calculations were made. Theory and experiment are in excellent agreement although the experimental data tend to be slightly above the theory. This is consistent with the usual boundary-layer displacement effect. At $x/R_n = 20$ the blunt-cone pressure is very nearly equal to the pointed-cone value shown on the far right of figure 19.

Flow properties off the body surface are most easily studied experimentally by means of the impact or pitot pressure, as shown in figure 20. The pitot-pressure distribution normal to the body is presented for all 7 meridional planes and for an axial station of $x_b/R_n = 16.7$. The theory extends all the way to the shock in each case, while the data do not, except for $\Phi = 60°$ and $\Phi = 150°$ where experimental shock positions are indicated by a sharp drop in pressure.

In the viscous boundary layer the pitot pressure is low, going to zero at the body surface. Evidence of a very thick viscous layer is indicated by the experimental data for the lee side of the body, $\Phi = 0$ and 30°. On the remaining meridional planes the boundary layer is very thin. The entropy layer is clearly indicated in the experimental data by the peak in the pitot pressure just off the windward side of the body. The theory underpredicts the peak value because of the previously described smoothing employed in the calculation. A theoretical maximum of $C_{p_p} = 9.03$ for $\Phi = 180°$ is determined by the use of the total pressure at the calculated minimum shock angle (fig. 13).

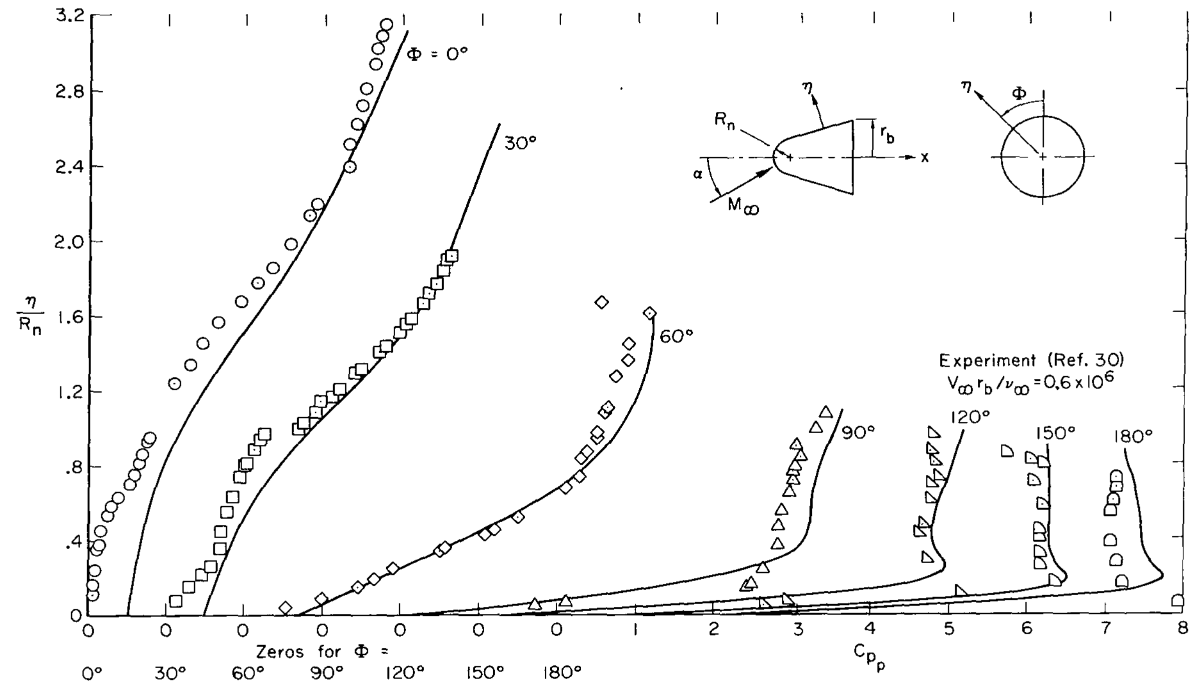

Figure 20.- Shock-layer pitot-pressure distribution; 15° sphere-cone, M_∞ = 10, α = 10°, x_B/R_n = 16.7.

Aside from the noted differences due to the boundary layer and the entropy layer, the proposed numerical method appears to give an adequate prediction of shock-layer properties.

CONCLUDING REMARKS

Characteristics theory for three-dimensional steady flow was reviewed and the compatibility equations were derived in terms of pressure and stream angles as dependent variables. It was argued that the major practical difficulty encountered in bicharacteristic methods results from the need for numerical differentiation and interpolation of randomly spaced data. Furthermore, it was observed that shock-layer coordinates are essential to a simple treatment of circumferential derivatives on the shock surface. A reference plane method was therefore adopted in which an equal number of points are equally spaced between the body and shock along each reference plane. This mesh introduces the added complication of nonorthogonal coordinates into the equations but allows the use of simpler numerical techniques.

With the constraint of a uniformly spaced mesh, particular characteristic lines are not followed as in more standard characteristics methods. The role of characteristics theory in the reference plane method is to determine how the finite difference equations are to be locally solved. Since the characteristics are not traced throughout the shock layer, the possible coalescence of waves to form embedded shocks is not determined during the calculation. However, characteristic lines can be traced afterward, from the numerical solution. Neglecting embedded shocks is not a serious deficiency since the calculations are correct for weak shocks (entropy rise being third-order in the deflection angle). In situations where strong shocks are suspected or known to occur (such as on flared bodies) special treatment would be required just as in standard two-dimensional methods.

Results for the three-dimensional flow around inclined blunted and pointed cones were presented to demonstrate the methods described and developed in this paper. Comparisons with a linearized characteristic method illustrated nonlinear angle-of-attack effects on crossflow parameters. Major effects of bluntness, which persist at large distances from the nose, were well predicted by the present methods. Predictions of surface and pitot pressures were found to be in good agreement with available experimental results for a 15° sphere-cone at 10° angle of attack.

While present examples were limited to bodies of revolution, the methods are not so restricted, being generally applicable to smooth bodies without axial symmetry. More complicated shapes typical of high-speed aircraft will require additional development, primarily in the area of special boundary conditions. For example, it should be possible, with special treatment of the leading-edge boundary condition, to calculate the flow over wings with supersonic leading edges. Finally, while there are no inherent limitations in angle of attack, it is clear that the flow near the leeward meridian must become wake-like at a sufficiently large inclination. In this case, it is essential to include the effects of viscosity and possible secondary shocks.

Ames Research Center
National Aeronautics and Space Administration
Moffett Field, Calif., 94035, July 7, 1969

APPENDIX A

DIRECTION COSINES FOR NONORTHOGONAL COORDINATES

In the derivation of the compatibility equations for the reference plane method it was necessary to transform from streamline coordinates to a nonorthogonal system consisting of s^*, η, and ζ. The direction s^* is the projection of the streamline on the meridional plane, η runs from body to shock in the meridional plane, and ζ is the out-of-plane direction (see fig. 3). This transformation is expressed as

$$\hat{x}_i = \varepsilon^*_{ij}\hat{z}_j^* \tag{A1}$$

where

$$\hat{x}_i = (\hat{s},\hat{n},\hat{t})$$

and

$$\hat{z}_j^* = (\hat{s}^*,\eta,\zeta)$$

It is the purpose of this appendix to write out the expressions for the direction consines ε^*_{ij}. The analysis is made for the more general ξ,η,ζ coordinates and is later specialized to the case where $\xi = s^*$.

The directions of the nonorthogonal ξ,η,ζ coordinates are determined step by step during the calculation as the shock shape is constructed (see section on Computational Procedure). When the location of the shock is known in terms of x,r,Φ, the locations of field points between the shock and body are also determined by the prescribed spacing of the points along the body normals. The direction cosines can then be obtained by numerical differentiation as described below. This process is described for the shock wave but applies generally to each ζ curve.

Let the shock surface be given by

$$r_s = r_s(x,\Phi) \tag{A2}$$

The intersection of the coordinate surface ξ = constant with the shock surface defines a curved line in space (a ζ curve; see fig. 3). The x,r coordinates of this space curve depend on the meridional angle, Φ, and on the body station, x_b, which locates the ξ = constant surface. For each body station this dependence is denoted by

$$x_s = \tilde{x}_s(\Phi) \tag{A3a}$$

$$r_s = \tilde{r}_s(\Phi) \tag{A3b}$$

Equations (A3a) and (A3b) define two angles

$$\tan \Delta x = \frac{1}{r_s} \frac{d\tilde{x}_s}{d\Phi} \tag{A4}$$

$$\tan \Delta r = \frac{1}{r_s} \frac{d\tilde{r}_s}{d\Phi} \tag{A5}$$

which can be evaluated numerically. (The Fourier method previously described is used.) In figure 21 the unit vector $\hat{\zeta}$ is related to $\hat{e}_\Phi$ through two rotations, the first rotation by Δx and the second by $\tilde{\delta}$. It may also be verified from this figure that

$$\tan \tilde{\delta} = \frac{dr}{r\, d\Phi} \cos \Delta x$$

and, by equation (A4),

$$\tan \tilde{\delta} = \tan \Delta r \cos \Delta x \tag{A6}$$

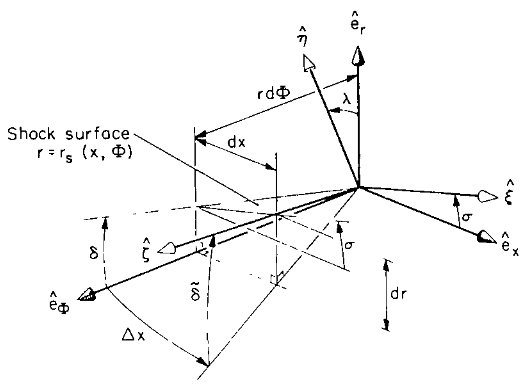

Figure 21.- Coordinate vectors and angles.

The remaining two unit vectors are defined by angles λ and σ; $\hat{\eta}$ is rotated by λ from $\hat{e}_r$ and $\hat{\xi}$ is rotated by σ from $\hat{e}_x$. Thus, one may write

$$\hat{\xi} = \cos \sigma\, \hat{e}_x + \sin \sigma\, \hat{e}_r \tag{A7}$$

$$\hat{\eta} = -\sin \lambda\, \hat{e}_x + \cos \lambda\, \hat{e}_r \tag{A8}$$

$$\hat{\zeta} = \cos \tilde{\delta} \sin \Delta x\, \hat{e}_x + \sin \tilde{\delta}\, \hat{e}_r + \cos \tilde{\delta} \cos \Delta x\, \hat{e}_\Phi \tag{A9}$$

The angle λ, which determines the direction of $\hat{\eta}$, may be arbitrarily specified. It is usually selected so that $\hat{\eta}$ is normal to the body surface. The angles σ and $\tilde{\delta}$ are determined at the shock by the calculated shock shape, and at the body by the given body shape. At intermediate points between the body and shock, σ and $\tilde{\delta}$ can be similarly calculated from the x,r,Φ coordinates of the mesh points. These coordinates are known for any specified mesh spacing once the shock position is determined.

It must be noted, however, that $\tilde{\delta}$ is distinct from the angle δ which is used in the shock conditions developed in appendix B. From figure 21 it is found that

$$\left.\begin{aligned} \tan \delta &= \frac{dr - dx \tan \sigma}{r\, d\Phi} \\ \text{or} \qquad \tan \delta &= \tan \Delta r - \tan \sigma \tan \Delta x \end{aligned}\right\} \tag{A10}$$

When $\hat{\eta}$ is chosen to be normal to the body axis, $\Delta x = 0$ and $\delta = \tilde{\delta}$.

Having specified the directions of $\hat{\xi},\hat{\eta},\hat{\zeta}$ by equations (A7), (A8), and (A9), the task of determining ε^*_{ij}, appearing in equation (A1), can now be completed. Equations (A7), (A8), and (A9) are more conveniently written with index notation as

$$\hat{z}_i = \bar{\nu}_{ij}\hat{X}_j \tag{A11}$$

where

$$\bar{\nu}_{ij} = \begin{pmatrix} \cos\sigma & \sin\sigma & 0 \\ -\sin\lambda & \cos\lambda & 0 \\ \cos\tilde{\delta}\sin\Delta x & \sin\tilde{\delta} & \cos\delta\cos\Delta x \end{pmatrix} \tag{A12}$$

The inverse transformation may be written

$$\hat{X}_i = \nu_{ij}\hat{z}_j \tag{A13}$$

where

$$\nu_{ij} = (\bar{\nu}_{ij})^{-1}$$

Although the matrix inversion can be performed numerically, for this problem it is more efficient to do the algebra beforehand, once and for all. This is done by taking scalar products of equation (A11) with $\hat{X}_j$ to obtain terms like $\hat{z}_1 \cdot \hat{X}_1 = \bar{\nu}_{11}$, $\hat{z}_1 \cdot \hat{X}_2 = \bar{\nu}_{12}$, and so on. On the other hand, the scalar products of equation (A13) with $\hat{z}_j$ give expressions such as

$$\hat{z}_1 \cdot \hat{X}_1 = \nu_{11} + \nu_{12}(\hat{\xi}\cdot\hat{\eta}) + \nu_{13}(\hat{\xi}\cdot\hat{\zeta})$$

$$\hat{z}_2 \cdot \hat{X}_1 = \nu_{11}(\hat{\eta}\cdot\hat{\xi}) + \nu_{12} + \nu_{13}(\hat{\eta}\cdot\hat{\zeta})$$

and so on. In this way, one obtains nine equations for the nine unknowns ν_{ij}. The solution of this set of equations by Cramer's rule can be formally written as (see, e.g., ref. 18)

$$\nu_{ij} = \frac{\bar{\nu}_{li} f_{lj}}{D} \tag{A14}$$

where f_{lj} represents the cofactor matrix of the coefficients of ν_{ij}.

$$f_{lj} = \begin{pmatrix} [1-(\hat{\eta}\cdot\hat{\zeta})^2] & [(\hat{\xi}\cdot\hat{\zeta})(\hat{\eta}\cdot\hat{\zeta})-(\hat{\xi}\cdot\hat{\eta})] & [(\hat{\xi}\cdot\hat{\eta})(\hat{\eta}\cdot\hat{\zeta})-(\hat{\xi}\cdot\hat{\zeta})] \\ f_{21} & [1-(\hat{\xi}\cdot\hat{\zeta})^2] & [(\hat{\xi}\cdot\hat{\eta})(\hat{\xi}\cdot\hat{\zeta})-(\hat{\eta}\cdot\hat{\zeta})] \\ f_{31} & f_{32} & [1-(\hat{\xi}\cdot\hat{\eta})^2] \end{pmatrix} \tag{A15}$$

where

$$f_{lj} = f_{jl}$$

and the determinant D is given by

$$D = 1 - (\hat{\eta} \cdot \hat{\zeta})^2 - (\hat{\xi} \cdot \hat{\eta})^2 - (\hat{\xi} \cdot \hat{\zeta})^2 - 2(\hat{\xi} \cdot \hat{\eta})(\hat{\xi} \cdot \hat{\zeta})(\hat{\eta} \cdot \hat{\zeta}) \quad \text{(A16)}$$

Equation (A14) provides the direction cosines between ξ,η,ζ and x,r,Φ coordinates. The corresponding relationships with s,n,t coordinates are obtained by use of equations (7), (8), and (9) which express the streamline directions in terms of $\hat{e}_x$, $\hat{e}_r$, $\hat{e}_\Phi$ and may be written

$$\hat{x}_i = \tau_{ij}\hat{X}_j \quad \text{(A17)}$$

where

$$\tau_{ij} = \begin{pmatrix} \cos\phi\cos\theta & \cos\phi\sin\theta & \sin\phi \\ -\sin\theta & \cos\theta & 0 \\ -\sin\phi\cos\theta & -\sin\phi\sin\theta & \cos\theta \end{pmatrix} \quad \text{(A18)}$$

The substitution of equation (A13) into (A17) yields

$$\hat{x}_i = \varepsilon_{ik}\hat{z}_k \quad \text{(A19)}$$

where ε_{ik} is obtained from

$$\varepsilon_{ik} = \tau_{ij}\nu_{jk} \quad \text{(A20)}$$

Equation (A20) gives the direction cosines between ξ,η,ζ and s,n,t coordinates. The explicit expressions for these direction cosines are involved, so the final combination of terms indicated by equation (A20) is left for the computer. The procedure is as follows. The matrix $\overline{\nu}_{ij}$, defined by (A12), is calculated with equations (A4), (A5), and (A6). The various scalar products in equations (A15) and (A16) are calculated from $\overline{\nu}_{ij}$, and the matrix ν_{ij} is then calculated from equation (A14). Finally, ε_{ik} is determined from equations (A18) and (A20).

The procedure described applies to general nonorthogonal coordinates ξ,η,ζ. The transformation used in equation (36) is a special case where the ξ direction is the streamline projection s^*. In this case, equation (A9) is replaced by

$$\hat{s}^* = \cos\theta\ \hat{e}_x + \sin\theta\ \hat{e}_r \tag{A21}$$

Then the subsequent relations will be modified accordingly and there is obtained

$$\varepsilon^*_{ik} = \tau_{ij}\nu^*_{jk} \tag{A22}$$

which determines the desired transformation relationship indicated by equation (A1).

APPENDIX B

SHOCK-BOUNDARY CONDITIONS FOR THREE-DIMENSIONAL FLOW

Consider an elemental portion of the shock surface with an outer unit normal $\hat{N}$, as shown in figure 22, and with unit vectors $\hat{T}$ and $\hat{L}$ completing an orthogonal set. The tangent vector $\hat{T}$ can be chosen such that the N-T plane is parallel to the direction of the free-stream velocity. This choice will permit evaluation of the jump conditions in the N-T plane with two-dimensional shock relations. Let $\hat{s}_\infty$ be a unit vector parallel to the free-stream velocity vector and with components

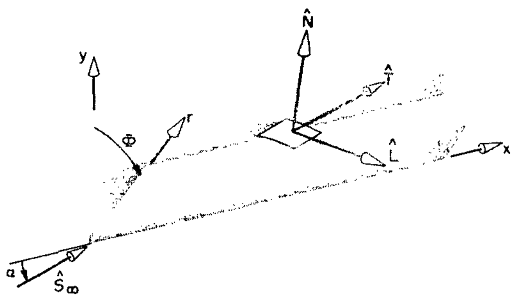

Figure 22.- Shock-wave normal and tangent vectors.

$$\hat{s}_\infty = \cos\alpha\,\hat{e}_x + \sin\alpha\cos\Phi\,\hat{e}_r - \sin\alpha\sin\Phi\,\hat{e}_\Phi \tag{B1}$$

in a cylindrical coordinate frame. The desired tangent vector $\hat{T}$ can be constructed from $\hat{s}_\infty$ and $\hat{N}$ by means of two vector- or cross-products. The first product

$$a\hat{L} = \hat{s}_\infty \times \hat{N} \tag{B2}$$

produces a vector parallel to $\hat{L}$, and the second product

$$\hat{T} = \hat{N}\times\hat{L} \tag{B3}$$

results in a vector which is normal to both $\hat{N}$ and $\hat{L}$, and which lies in the s_∞-N plane. The factor a in equation (B2) is equal to the sine of the angle between $\hat{s}_\infty$ and $\hat{N}$ and may be evaluated from the scalar product

$$b = \hat{s}_\infty \cdot \hat{N} = \cos(s_\infty, N) \tag{B4}$$

to give

$$a = \sqrt{1 - b^2} = \sqrt{1 - (\hat{s}_\infty \cdot \hat{N})^2} \tag{B5}$$

Combining equations (B2) and (B3) and expanding the resulting vector triple product one obtains

$$\left.\begin{aligned} \hat{T} &= \frac{1}{a}\left[\hat{N}\times(\hat{s}_\infty \times \hat{N})\right] \\ &\text{or} \\ \hat{T} &= \frac{1}{a}(\hat{s}_\infty - b\hat{N}) \end{aligned}\right\} \tag{B6}$$

In terms of components T_x, T_r, and T_Φ, equation (B6) becomes

$$\hat{T} = \left(\frac{s_x - bN_x}{a}\right)\hat{e}_x + \left(\frac{s_r - bN_r}{a}\right)\hat{e}_r + \left(\frac{s_\Phi - bN_\Phi}{a}\right)\hat{e}_\Phi \qquad (B7)$$

Equation (B7) permits evaluation of the true inclination of the shock surface, and therefore allows the jump conditions to be determined with standard planar shock relations (see, e.g., ref. 32). The angle σ' between $\hat{s}_\infty$ and $\hat{T}$ is given by

$$\left.\begin{aligned} \cos\sigma' &= \hat{s}_\infty \cdot \hat{T} \\ &\text{or} \\ \cos\sigma' &= s_x T_x + s_r T_r + s_\Phi T_\Phi \end{aligned}\right\} \qquad (B8)$$

In the following development σ' is expressed in terms of two angles measured in the cylindrical coordinates.

Let σ be the angle between $\hat{e}_x$ and the trace of the shock surface on the plane Φ = constant, and let δ be the angle between $\hat{e}_\Phi$ and the shock trace on the plane x = constant as illustrated in figure 23. The shock angle δ is obtained by numerical differentiation as described in appendix A (see eq. (A10) and fig. 21). It is easily verified that the following relations hold between the angles shown in figure 23.

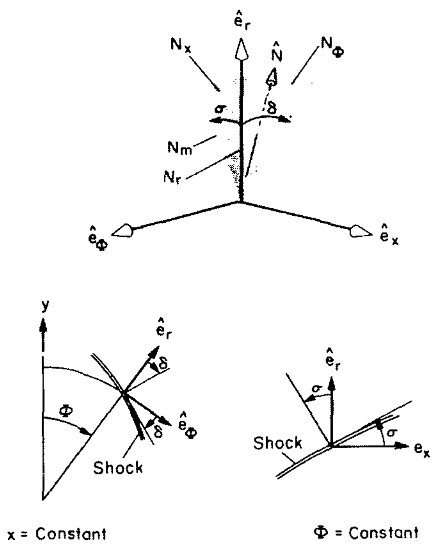

Figure 23.- Shock angles.

$$N_x = -N_m \sin\sigma \qquad (B9)$$

$$N_r = N_m \cos\sigma \qquad (B10)$$

$$N_\Phi = -N_m \cos\sigma \tan\delta \qquad (B11)$$

where N_m is the projection of $\hat{N}$ on the x-r plane and satisfies the relation

$$N_m^2 + N_\Phi^2 = 1$$

Substitution of N_Φ from equation (B11) gives

$$N_m = \frac{1}{\sqrt{1 + \cos^2\sigma \tan^2\delta}} \qquad (B12)$$

and the shock normal vector may finally be written in terms of σ and δ as

$$\hat{N} = \frac{(-\sin\sigma\,\hat{e}_x + \cos\sigma\,\hat{e}_r - \cos\sigma\tan\delta\,\hat{e}_\Phi)}{\sqrt{1 + \cos^2\sigma\tan^2\delta}} \tag{B13}$$

The true shock angle can now be evaluated in terms of σ and δ by equations (B1), (B7), (B8), and (B13), and the jump conditions can be calculated.

It is now necessary to determine the flow angles θ and ϕ measured relative to the meridional planes.

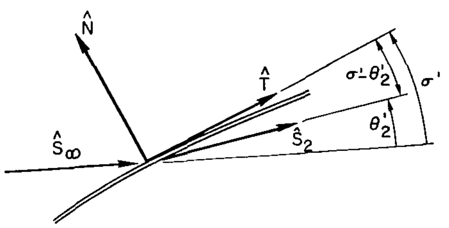

Figure 24.- Shock and flow angles in the n-t plane.

The streamline direction, measured in the N-T plane (fig. 24), is turned from the free stream by the angle θ_2'. Since the streamline tangent $\hat{s}_2$ lies, by definition, in the N-T plane, one may write

$$\hat{s}_2 = -\sin(\sigma' - \theta_2')\hat{N} + \cos(\sigma' - \theta_2')\hat{T} \tag{B14}$$

Using equations (B7) and (B13), the vectors $\hat{N}$ and $\hat{T}$ can be written in terms of their components to give

$$\hat{s}_2 = (AN_x + BT_x)\hat{e}_x + (AN_r + BT_r)\hat{e}_r + (AN_\Phi + BT_\Phi)\hat{e}_\Phi \tag{B15}$$

where

$$A = -\sin(\sigma' - \theta_2')$$

$$B = \cos(\sigma' - \theta_2')$$

Equation (7), on the other hand, gives $\hat{s}_2$ in terms of θ and ϕ as follows:

$$\hat{s}_2 = \cos\phi_2\cos\theta_2\,\hat{e}_x + \cos\phi_2\sin\theta_2\,\hat{e}_r + \sin\phi_2\,\hat{e}_\Phi \tag{B16}$$

Thus, by equating components of equations (B15) and (B16) one obtains finally

$$\tan\theta = \frac{-\sin(\sigma' - \theta_2')N_r + \cos(\sigma' - \theta_2')T_r}{-\sin(\sigma' - \theta_2')N_x + \cos(\sigma' - \theta_2')T_x} \tag{B17}$$

and

$$\sin\phi = -\sin(\sigma' - \theta_2')N_\Phi + \cos(\sigma' - \theta_2')T_\Phi \tag{B18}$$

If for given free-stream conditions, p_∞, ρ_∞, V_∞, the standard planar shock conditions are written in the form (see ref. 32):

$$\left.\begin{aligned} p &= p(\sigma') \\ \rho &= \rho(\sigma') \\ \theta &= \theta(\sigma') \end{aligned}\right\} \tag{B19}$$

then the equations developed in this appendix allow the three-dimensional shock conditions to be functionally written as

$$\left.\begin{aligned} p &= \tilde{p}(\sigma;\delta,\Phi,\alpha) \\ \rho &= \tilde{\rho}(\sigma;\delta,\Phi,\alpha) \\ \theta &= \tilde{\theta}(\sigma;\delta,\Phi,\alpha) \\ \phi &= \tilde{\phi}(\sigma;\delta,\Phi,\alpha) \end{aligned}\right\} \tag{B20}$$

This is the form of the shock conditions employed in equation (62).

The overall shock calculation is performed in a straightforward iterative manner. This procedure is started with known field data, including σ and δ, on an initial data surface. A shock point on the new data surface is determined by the average value of σ between the initial and new shock points,

$$\bar{\sigma} = 1/2(\sigma_1 + \sigma_2)$$

To begin, σ_2 is set equal to σ_1 and then subsequent estimates are made (either by the Newton method or by the bisecting method) until the pressure from equation (B20) agrees with the pressure calculated from the compatibility equation (57). During each iteration the current value of $\sigma = \sigma_2$ and the old value of $\delta = \delta_1$ are used to determine the true shock angle σ' by equation (B8). The pressure and other variables are then calculated from equations (B19). When this has been done for all the shock points on the new data surface, new values for δ can be determined by numerical differentiation with respect to Φ as described in appendix A. The entire process can then be repeated to refine the results; this is discussed in the section on Global Iteration.

APPENDIX C

SURFACE BOUNDARY CONDITIONS FOR BODIES WITHOUT AXIAL SYMMETRY

For noncircular bodies the surface boundary is complicated by the fact that the surface normal is not in the meridional plane. This means the boundary condition will involve both flow angles θ and ϕ. (In terms of velocities, all three components, u, v, w, enter into the conditions since none of the components are parallel to the body surface.) In this appendix the boundary condition for θ, which was given previously in equation (61a), is derived from the tangency condition on the velocity vector.

Let the equation of the body be given by

$$g(x,r,\Phi) = r - f(x,\Phi) \tag{C1}$$

The unit outer normal to the surface may be expressed

$$\hat{N} = \frac{\nabla g}{|\nabla g|} \tag{C2}$$

where ∇ is the vector gradient operator. In terms of cylindrical coordinates, one obtains

$$\hat{N} = \frac{-\frac{\partial f}{\partial x}\hat{e}_x + \hat{e}_r - \frac{1}{r}\frac{\partial f}{\partial \Phi}\hat{e}_\Phi}{\sqrt{1 + \left(\frac{\partial f}{\partial x}\right)^2 + \left(\frac{1}{r}\frac{\partial f}{\partial \Phi}\right)^2}} \tag{C3}$$

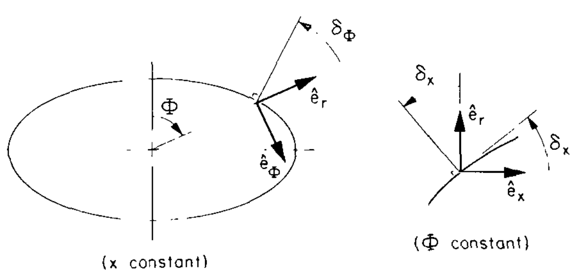

Figure 25.- Surface inclination angles.

The derivatives of f in equation (C3) are related to the surface inclination angles, figure 25, according to

$$\tan \delta_x = \left(\frac{\partial f}{\partial x}\right)_\Phi \tag{C4}$$

and

$$\tan \delta_\Phi = \frac{1}{r}\left(\frac{\partial f}{\partial \Phi}\right)_x \tag{C5}$$

From equation (7) the streamline direction is expressed in terms of flow angles θ and ϕ

$$\hat{s} = \cos\phi\cos\theta\,\hat{e}_x + \cos\phi\sin\theta\,\hat{e}_r + \sin\phi\,\hat{e}_\Phi \tag{C6}$$

The tangency condition, $\hat{s} \cdot \hat{N} = 0$, may now be obtained from the scalar product of equations (C3) and (C6). This gives

$$N_x \cos \phi \cos \theta + N_r \cos \phi \sin \theta + N_\Phi \sin \phi = 0 \qquad \text{(C7)}$$

where N_x, N_r, N_Φ are the components of $\hat{N}$ along $\hat{e}_x$, $\hat{e}_r$, $\hat{e}_\Phi$, and are identified by equation (C3). Equation (C7) may be written as a quadratic relation in $\tan \theta$

$$(N_r^2 - N_\Phi^2 \tan^2 \phi)\tan^2 \theta + 2N_x N_r \tan \theta + (N_x^2 - N_\Phi^2 \tan^2 \phi) = 0 \qquad \text{(C8)}$$

The solution is

$$\tan \theta = \frac{\left[-\frac{N_x}{N_r} \pm \frac{N_\Phi \tan \phi}{N_r} \sqrt{1 + \left(\frac{N_x}{N_r}\right)^2 - \left(\frac{N_\phi}{N_r}\right)^2 \tan^2 \phi}\right]}{[1 - (N_\Phi/N_r)^2 \tan^2 \phi]} \qquad \text{(C9)}$$

Rewriting equation (C9) in terms of the surface inclination angles given by equations (C4) and (C5), one obtains

$$\tan \theta = \frac{\left(\tan \delta_x + \tan \delta_\Phi \tan \phi \sqrt{1 + \tan^2 \delta_x - \tan^2 \delta_\Phi \tan^2 \phi}\right)}{(1 - \tan^2 \delta_\Phi \tan^2 \phi)} \qquad \text{(C10)}$$

where the positive root is chosen so that θ is decreased when $\phi < 0$ and $\delta_\Phi > 0$.

Equations (C10), (C4), and (C5) determine the flow angle θ in terms of the crossflow angle ϕ and the body geometry. It is easily verified that for zero crossflow, $\phi = 0$, equation (C10) reduces to

$$\tan \theta = \tan \delta_x$$

which is the usual condition for circular bodies.

REFERENCES

1. Courant, R.; and Friedrichs, K. O.: Supersonic Flow and Shock Waves. Interscience, New York, 1948.

2. Courant, R.; and Hilbert, D.: Methods of Mathematical Physics. Vol. II Partial Differential Equations. Interscience, New York, 1962.

3. Ferri, Antonio: Characteristics Methods for Problems in Three Independent Variables. Ch. 5, sec. G of General Theory of High Speed Aerodynamics, W. R. Sears, ed., Princeton University Press, 1954, pp. 642, 657.

4. Moretti, G.; Sanlorenzo, E. A.; Magnus, D. E.; and Weilerstein, G.: Flow Field Analysis of Reentry Configurations by a General Three-Dimensional Method of Characteristics. Air Force Systems Command, Aero. Systems Div., TR-67-727, vol. III, Feb. 1962.

5. Powers, S. A.; Niemann, A. F., Jr.; and Der, J., Jr.: A Numerical Procedure for Determining the Combined Viscid-Inviscid Flow Fields Over Generalized Three-Dimensional Bodies. Air Force Systems Command, AFFDL-TR-67-124, vol. I, Dec. 1967.

6. Strom, Charles R.: The Method of Characteristics for Three-Dimensional Real-Gas Flows. Final Report 1, Apr 1963-Nov. 1966. Air Force Systems Command, AFFDL-TR-67-47, July 1967.

7. Sauerwein, Harry: Numerical Calculation of Multidimensional and Unsteady Flows by the Method of Characteristics. J. Computational Phys., vol. 1, Feb. 1967, pp. 406-432.

8. Butler, D. S.: The Numerical Solution of Hyperbolic Systems of Partial Differential Equations in Three-Independent Variables. Proc. Roy. Soc. A 255, no. 1281, April 1960, pp. 232-252.

9. Katskova, O. N.; and Chushkin, P. I.: Three Dimensional Supersonic Equilibrium Flow of a Gas Around Bodies at Angle of Attack. NASA TT F-9790, 1965.

10. Ransom, V. H.; Thompson, H. D.; and Hoffman, J. D.: Analysis of Three-Dimensional Scramjet Exhaust Nozzle Flow Fields by a New Second-Order Method of Characteristics. AIAA Paper 69-5, presented at the Seventh Aerospace Sciences Meeting, Jan. 20-22, 1969.

11. Babenko, K. I.; Voskresenskiy, G. P.; Lyubimov, A. N.; and Rusanov, V. V.: Three-Dimensional Flow of Ideal Gas Past Smooth Bodies. NASA TT F-380, 1966.

12. Chushkin, P. I.: Numerical Method of Characteristics for Three-Dimensional Supersonic Flows. Prog. in Aeron. Sci., vol. 9, K. Küchemann, ed., Pergamon Press, 1968.

13. Rakich, John V.: Three-Dimensional Flow Calculation by the Method of Characteristics. AIAA J., vol. 5, no. 10, Oct. 1967, pp. 1906-1908.

14. Rakich, John V.; and Cleary, Joseph W.: Theoretical and Experimental Study of Supersonic Steady Flow Around Inclined Bodies of Revolution. Seventh Aerospace Sciences Meeting, Jan. 20-22, 1969, Paper 69-187.

15. Rakich, John V.: Numerical Calculation of Supersonic Flows of a Perfect Gas Over Bodies of Revolution at Small Angles of Yaw. NASA TN D-2390, 1964.

16. Chu, Chong-Wei: Compatibility Relations and a Generalized Finite Difference Approximation for Three-Dimensional Steady Supersonic Flow. AIAA J., vol. 5, no. 3, March 1967, pp. 493-501.

17. Fox, L.: Numerical Solution of Ordinary and Partial Differential Equations. Ch. 18 of Finite-Difference Methods for Hyperbolic Equations. Pergamon Press, 1962.

18. Hildebrand, F. B.: Introduction to Numerical Analysis. McGraw-Hill Book Co., Inc., 1956.

19. Hamming, Richard W.: Numerical Methods for Scientists and Engineers. McGraw-Hill Book Co., Inc., 1962.

20. Lomax, Harvard; and Inouye, Mamoru: Numerical Analysis of Flow Properties About Blunt Bodies Moving at Supersonic Speeds in an Equilibrium Gas. NASA TR R-204, 1964.

21. Briggs, Benjamin R.: The Numerical Calculation of Flow Past Conical Bodies Supporting Elliptic Conical Shock Waves at Finite Angles of Incidence. NASA TN D-340, 1960.

22. Moretti, G.: Inviscid Flow Field Past a Pointed Cone at an Angle of Attack. AIAA J., vol. 5, no. 4, April 1967, pp. 789-791.

23. Rakich, John V.: Calculation of Hypersonic Flow Over Bodies of Revolution at Small Angles of Attack. AIAA J., vol. 3, no. 3, March 1965, pp. 458-464.

24. Ferri, Antonio: Conical Flow. Ch. 3, sec. H of General Theory of High Speed Aerodynamics, W. R. Sears, ed., Princeton University Press, 1954.

25. Gonidou, René: Supersonic Flows Around Cones at Incidence. NASA TT F-11,473, 1967.

26. Lax, P.; and Wendroff, B.: Systems of Conservative Laws. Commun. Pure Appl. Math., vol. 13, May 1960, pp. 217-237.

27. Richtmyer, Robert D.: A Survey of Difference Methods for Non-Steady Fluid Dynamics. National Center for Atmospheric Research Technical Note 63-2, Boulder, Colorado, Aug. 1962.

28. Gallo, William F.; and Rakich, John V.: Investigation of Methods for Predicting Flow in the Shock Layer Over Bodies at Small Angles of Attack. NASA TN D-3946, 1967.

29. Inouye, Mamoru; Rakich, John V.; and Lomax, Harvard: A Description of Numerical Methods and Computer Programs for Two-Dimensional and Axisymmetric Supersonic Flow Over Blunt-Nosed and Flared Bodies. NASA TN D-2970, 1965.

30. Cleary, Joseph W.: An Experimental and Theoretical Investigation of the Pressure Distribution and Flow Fields of Blunted Cones at Hypersonic Mach Numbers. NASA TN D-2969, 1965.

31. Cleary, Joseph W.: Effects of Angle of Attack and Bluntness on the Shock-Layer Properties of a 15° Cone at a Mach Number of 10.6. NASA TN D-4909, 1968.

32. Ames Research Staff: Equations, Tables, and Charts for Compressible Flow. NACA Rep. 1135, 1953.

TABLE I.- EFFECT OF GLOBAL ITERATION ON SHOCK ANGLE

[15° sphere-cone; M = 10, α = 10°, 15 points and 7 planes]

(a) Calculation from $x/R_n = 2.0$ to $x/R_n = 3.0$

Plane, Φ, deg	Iterations	
	0	1
	σ, deg at $x/R_n = 3.0$	
0	29.0763	29.0763
30	27.6271	27.6275
60	23.7124	23.7137
90	18.8404	18.8417
120	15.5193	15.5194
150	14.2633	14.2633
180	13.9813	13.9813

(b) Calculation from $x/R_n = 10.0$ to $x/R_n = 11.0$

Plane, Φ, deg	Iterations	
	0	1
	σ, deg at $x/R_n = 11.0$	
0	21.2083	21.2083
30	19.5249	19.5273
60	16.1617	16.1651
90	16.0245	16.0260
120	17.4741	17.4756
150	17.4404	17.4407
180	17.4416	17.4415

TABLE II.- ACCURACY AND COMPUTING TIME

[15° sphere-cone; M = 10, α = 10°. Calculation from x/R_n = 2 to x/R_n = 3.]

(a) Shock angles and surface pressure on Φ = 90° plane, x/R_n = 3

Points	Planes								
	K = 3			K = 5			K = 7		
	σ	δ	p_b	σ	δ	p_b	σ	δ	p_b
J = 5	19.3114	-10.3313	840.42	19.5919	-10.1783	834.02	19.2893	-10.3555	828.85
J = 10	18.9847	-10.3961	861.15	18.9337	-10.5549	849.52	18.9318	-10.5644	849.36
J = 15	18.9138	-10.4090	864.56	18.8482	-10.6017	853.39	18.8404	-10.6294	853.44

(b) Computing time

Points	Planes								
	K = 3			K = 5			K = 7		
	Total points, N	Time, t, min	Unit time, t/N	Total points, N	Time, t, min	Unit time, t/N	Total points, N	Time, t, min	Unit time, t/N
J = 5	90	0.36	0.400×10^{-2}	150	0.57	0.380×10^{-2}	210	0.7	0.333×10^{-2}
J = 10	420	.75	$.179\times10^{-2}$	700	1.17	$.167\times10^{-2}$	980	1.70	$.174\times10^{-2}$
J = 15	1035	1.35	$.130\times10^{-2}$	1725	2.30	$.133\times10^{-2}$	2415	3.34	$.138\times10^{-2}$

TABLE III.- 15° POINTED CONE SOLUTION

PERFECT GAS
GAS CONSTANT = 0.17160E 04   GAMMA = 0.14000E 01
FREE-STREAM CONDITIONS
M= 0.10600E 02 V= 0.39662E 04 P= 0.10000E 01 RHO= 0.10000E-04 T= 0.58275E 02 H= 0.35000E 06 HT= 0.82152E 07
EQUISPACED STARTING DATA   11 POINTS   9 PLANES
PLANES EQUALLY SPACED
STARTING DATA NORMAL TO BODY SURFACE
ANGLE OF ATTACK = 10.00 DEG
CHARACTERISTIC METHOD
IN(21)= 0 COR, N22 = 0 ITR, IN(25)= 2 BC, INX(6)= 3 BODY DENSITY
FL(4)= 0.1800E 01 STEP SIZE, FL(8)= 0.1000E 01 SMOOTH

PLANE 1 ANGL = 0.00 DEG
LEEWARD PLANE
FIELD DATA
SHOCK ANGLES, DEG   SIGMA= 18.5124   DELTA= -0.0000

X	R	THETA	PHI	P	RHO	H	V	M	M*
0.98395E 00	0.32785E 00	0.24764E 00	-0.00000E-38	0.27055E 01	0.19796E-04	0.47836E 06	0.39337E 04	0.89927E 01	0.89927E 01
0.98555E 00	0.32186E 00	0.24945E 00	-0.00000E-38	0.27456E 01	0.19989E-04	0.48074E 06	0.39331E 04	0.89690E 01	0.89690E 01
0.98716E 00	0.31587E 00	0.25107E 00	-0.00000E-38	0.27781E 01	0.20145E-04	0.48267E 06	0.39326E 04	0.89499E 01	0.89499E 01
0.98876E 00	0.30988E 00	0.25257E 00	-0.00000E-38	0.28047E 01	0.20269E-04	0.48432E 06	0.39321E 04	0.89337E 01	0.89337E 01
0.99037E 00	0.30389E 00	0.25400E 00	-0.00000E-38	0.28266E 01	0.20366E-04	0.48577E 06	0.39318E 04	0.89196E 01	0.89196E 01
0.99197E 00	0.29790E 00	0.25543E 00	-0.00000E-38	0.28445E 01	0.20441E-04	0.48704E 06	0.39315E 04	0.89072E 01	0.89072E 01
0.99358E 00	0.29191E 00	0.25690E 00	-0.00000E-38	0.28589E 01	0.20505E-04	0.48799E 06	0.39312E 04	0.88980E 01	0.88980E 01
0.99518E 00	0.28592E 00	0.25844E 00	-0.00000E-38	0.28701E 01	0.20570E-04	0.48836E 06	0.39311E 04	0.88944E 01	0.88944E 01
0.99679E 00	0.27993E 00	0.25994E 00	-0.00000E-38	0.28786E 01	0.20640E-04	0.48813E 06	0.39312E 04	0.88966E 01	0.88966E 01
0.99839E 00	0.27394E 00	0.26116E 00	-0.00000E-38	0.28855E 01	0.20706E-04	0.48774E 06	0.39313E 04	0.89004E 01	0.89004E 01
0.10000E 01	0.26795E 00	0.26180E 00	-0.00000E-38	0.28922E 01	0.20762E-04	0.48757E 06	0.39313E 04	0.89021E 01	0.89021E 01

PLANE 2 ANGL = 22.50 DEG
FIELD DATA
SHOCK ANGLES, DEG   SIGMA= 18.5966   DELTA= 1.3917

X	R	THETA	PHI	P	RHO	H	V	M	M*
0.98339E 00	0.32995E 00	0.24898E 00	-0.69236E-01	0.32071E 01	0.21986E-04	0.51055E 06	0.39255E 04	0.86864E 01	0.86659E 01
0.98505E 00	0.32375E 00	0.24930E 00	-0.69743E-01	0.31767E 01	0.21793E-04	0.51019E 06	0.39256E 04	0.86897E 01	0.86689E 01
0.98671E 00	0.31755E 00	0.24990E 00	-0.70020E-01	0.31529E 01	0.21615E-04	0.51052E 06	0.39255E 04	0.86867E 01	0.86657E 01
0.98837E 00	0.31135E 00	0.25075E 00	-0.70021E-01	0.31339E 01	0.21439E-04	0.51163E 06	0.39252E 04	0.86767E 01	0.86557E 01
0.99003E 00	0.30515E 00	0.25182E 00	-0.69673E-01	0.31182E 01	0.21239E-04	0.51385E 06	0.39246E 04	0.86567E 01	0.86360E 01
0.99169E 00	0.29895E 00	0.25312E 00	-0.68884E-01	0.31043E 01	0.20962E-04	0.51832E 06	0.39235E 04	0.86168E 01	0.85966E 01
0.99335E 00	0.29275E 00	0.25461E 00	-0.67720E-01	0.30911E 01	0.20447E-04	0.52910E 06	0.39207E 04	0.85225E 01	0.85032E 01
0.99501E 00	0.28655E 00	0.25629E 00	-0.66943E-01	0.30774E 01	0.19309E-04	0.55781E 06	0.39134E 04	0.82848E 01	0.82665E 01
0.99668E 00	0.28035E 00	0.25811E 00	-0.68538E-01	0.30619E 01	0.17025E-04	0.62948E 06	0.38951E 04	0.77623E 01	0.77444E 01
0.99834E 00	0.27415E 00	0.26000E 00	-0.74793E-01	0.30438E 01	0.13579E-04	0.78452E 06	0.38550E 04	0.68817E 01	0.68629E 01
0.10000E 01	0.26795E 00	0.26180E 00	-0.85422E-01	0.30238E 01	0.10202E-04	0.10374E 07	0.37889E 04	0.58817E 01	0.58609E 01

PLANE 3 ANGL = 45.00 DEG
FIELD DATA
SHOCK ANGLES, DEG   SIGMA= 18.5775   DELTA= -1.5278

X	R	THETA	PHI	P	RHO	H	V	M	M*
0.98331E 00	0.33025E 00	0.25504E 00	-0.12197E 00	0.50977E 01	0.28462E-04	0.62687E 06	0.38957E 04	0.77798E 01	0.77230E 01
0.98497E 00	0.32402E 00	0.25413E 00	-0.12138E 00	0.49424E 01	0.27594E-04	0.62689E 06	0.38957E 04	0.77797E 01	0.77234E 01
0.98664E 00	0.31779E 00	0.25357E 00	-0.12055E 00	0.48026E 01	0.26739E-04	0.62864E 06	0.38953E 04	0.77680E 01	0.77125E 01
0.98831E 00	0.31156E 00	0.25335E 00	-0.11942E 00	0.46769E 01	0.25879E-04	0.63253E 06	0.38943E 04	0.77420E 01	0.76878E 01
0.98998E 00	0.30533E 00	0.25349E 00	-0.11793E 00	0.45640E 01	0.24991E-04	0.63918E 06	0.38926E 04	0.76983E 01	0.76457E 01
0.99165E 00	0.29910E 00	0.25399E 00	-0.11604E 00	0.44624E 01	0.24043E-04	0.64960E 06	0.38899E 04	0.76311E 01	0.75806E 01
0.99332E 00	0.29287E 00	0.25485E 00	-0.11385E 00	0.43708E 01	0.22985E-04	0.66556E 06	0.38858E 04	0.75311E 01	0.74831E 01
0.99499E 00	0.28664E 00	0.25608E 00	-0.11203E 00	0.42875E 01	0.21705E-04	0.69138E 06	0.38791E 04	0.73764E 01	0.73310E 01
0.99666E 00	0.28041E 00	0.25766E 00	-0.11237E 00	0.42097E 01	0.19913E-04	0.73992E 06	0.38666E 04	0.71073E 01	0.70633E 01
0.99833E 00	0.27418E 00	0.25959E 00	-0.11741E 00	0.41346E 01	0.17061E-04	0.84818E 06	0.38385E 04	0.65900E 01	0.65456E 01
0.10000E 01	0.26795E 00	0.26180E 00	-0.12786E 00	0.40623E 01	0.12596E-04	0.11287E 07	0.37647E 04	0.56028E 01	0.55585E 01

PLANE 4 ANGL = 67.50 DEG
FIELD DATA
SHOCK ANGLES, DEG   SIGMA= 18.2994   DELTA= -2.5439

X	R	THETA	PHI	P	RHO	H	V	M	M*
0.98464E 00	0.32526E 00	0.25140E 00	-0.15815E 00	0.82016E 01	0.35355E-04	0.81193E 06	0.38479E 04	0.67521E 01	0.66697E 01
0.98618E 00	0.31953E 00	0.25099E 00	-0.15560E 00	0.79933E 01	0.34195E-04	0.81815E 06	0.38463E 04	0.67236E 01	0.66440E 01
0.98771E 00	0.31380E 00	0.25086E 00	-0.15280E 00	0.78012E 01	0.33049E-04	0.82617E 06	0.38442E 04	0.66872E 01	0.66109E 01
0.98925E 00	0.30806E 00	0.25103E 00	-0.14971E 00	0.76251E 01	0.31909E-04	0.83637E 06	0.38416E 04	0.66417E 01	0.65690E 01
0.99079E 00	0.30233E 00	0.25150E 00	-0.14630E 00	0.74638E 01	0.30759E-04	0.84930E 06	0.38382E 04	0.65852E 01	0.65164E 01
0.99232E 00	0.29660E 00	0.25228E 00	-0.14252E 00	0.73160E 01	0.29566E-04	0.86607E 06	0.38338E 04	0.65137E 01	0.64491E 01
0.99386E 00	0.29087E 00	0.25339E 00	-0.13845E 00	0.71800E 01	0.28239E-04	0.88991E 06	0.38276E 04	0.64154E 01	0.63554E 01
0.99539E 00	0.28514E 00	0.25484E 00	-0.13460E 00	0.70548E 01	0.26552E-04	0.92994E 06	0.38171E 04	0.62586E 01	0.62034E 01
0.99693E 00	0.27941E 00	0.25670E 00	-0.13230E 00	0.69389E 01	0.24175E-04	0.10046E 07	0.37975E 04	0.59907E 01	0.59398E 01
0.99846E 00	0.27368E 00	0.25901E 00	-0.13318E 00	0.68305E 01	0.21092E-04	0.11335E 07	0.37634E 04	0.55892E 01	0.55413E 01
0.10000E 01	0.26795E 00	0.26180E 00	-0.13705E 00	0.67275E 01	0.18061E-04	0.13037E 07	0.37179E 04	0.51485E 01	0.51020E 01

TABLE III.- 15° POINTED CONE SOLUTION - Concluded

PLANE 5 ANGL = 90.00 DEG
FIELD DATA
SHOCK ANGLES, DEG SIGMA= 18.0106 DELTA= -2.3858

X	R	THETA	PHI	P	RHO	H	V	M	M*
0.98591E 00	0.32052E 00	0.24054E 00	-0.17324E 00	0.12522E 02	0.41104E-04	0.10663E 07	0.37812E 04	0.57899E 01	0.57058E 01
0.98732E 00	0.31526E 00	0.24160E 00	-0.16915E 00	0.12337E 02	0.40064E-04	0.10778E 07	0.37782E 04	0.57542E 01	0.56744E 01
0.98873E 00	0.31000E 00	0.24287E 00	-0.16489E 00	0.12162E 02	0.39019E-04	0.10910E 07	0.37747E 04	0.57141E 01	0.56388E 01
0.99014E 00	0.30475E 00	0.24433E 00	-0.16042E 00	0.11996E 02	0.37958E-04	0.11061E 07	0.37707E 04	0.56687E 01	0.55982E 01
0.99155E 00	0.29949E 00	0.24599E 00	-0.15575E 00	0.11838E 02	0.36868E-04	0.11238E 07	0.37660E 04	0.56169E 01	0.55517E 01
0.99296E 00	0.29423E 00	0.24786E 00	-0.15085E 00	0.11688E 02	0.35739E-04	0.11446E 07	0.37605E 04	0.55576E 01	0.54964E 01
0.99436E 00	0.28898E 00	0.24997E 00	-0.14568E 00	0.11544E 02	0.34566E-04	0.11689E 07	0.37540E 04	0.54899E 01	0.54336E 01
0.99577E 00	0.28372E 00	0.25235E 00	-0.14026E 00	0.11408E 02	0.33317E-04	0.11984E 07	0.37461E 04	0.54107E 01	0.53593E 01
0.99718E 00	0.27846E 00	0.25506E 00	-0.13503E 00	0.11277E 02	0.31777E-04	0.12421E 07	0.37345E 04	0.52981E 01	0.52515E 01
0.99859E 00	0.27321E 00	0.25818E 00	-0.13121E 00	0.11151E 02	0.29391E-04	0.13279E 07	0.37114E 04	0.50924E 01	0.50502E 01
0.10000E 01	0.26795E 00	0.26180E 00	-0.12965E 00	0.11030E 02	0.25711E-04	0.15015E 07	0.36643E 04	0.47282E 01	0.46903E 01

PLANE 6 ANGL =112.50 DEG
FIELD DATA
SHOCK ANGLES, DEG SIGMA= 17.7465 DELTA= -1.9369

X	R	THETA	PHI	P	RHO	H	V	M	M*
0.98719E 00	0.31577E 00	0.22634E 00	-0.16273E 00	0.17628E 02	0.45187E-04	0.13654E 07	0.37013E 04	0.50083E 01	0.49448E 01
0.98847E 00	0.31099E 00	0.22929E 00	-0.15826E 00	0.17593E 02	0.44637E-04	0.13795E 07	0.36975E 04	0.49776E 01	0.49177E 01
0.98975E 00	0.30620E 00	0.23230E 00	-0.15365E 00	0.17547E 02	0.44049E-04	0.13942E 07	0.36935E 04	0.49459E 01	0.48898E 01
0.99103E 00	0.30142E 00	0.23539E 00	-0.14886E 00	0.17492E 02	0.43428E-04	0.14097E 07	0.36893E 04	0.49130E 01	0.48607E 01
0.99231E 00	0.29664E 00	0.23860E 00	-0.14386E 00	0.17431E 02	0.42774E-04	0.14263E 07	0.36848E 04	0.48784E 01	0.48300E 01
0.99359E 00	0.29186E 00	0.24193E 00	-0.13859E 00	0.17363E 02	0.42076E-04	0.14443E 07	0.36799E 04	0.48415E 01	0.47970E 01
0.99487E 00	0.28708E 00	0.24543E 00	-0.13299E 00	0.17288E 02	0.41296E-04	0.14653E 07	0.36742E 04	0.47993E 01	0.47586E 01
0.99616E 00	0.28229E 00	0.24913E 00	-0.12706E 00	0.17210E 02	0.40302E-04	0.14946E 07	0.36662E 04	0.47416E 01	0.47050E 01
0.99744E 00	0.27751E 00	0.25305E 00	-0.12095E 00	0.17127E 02	0.38857E-04	0.15427E 07	0.36531E 04	0.46503E 01	0.46179E 01
0.99872E 00	0.27273E 00	0.25724E 00	-0.11478E 00	0.17038E 02	0.36921E-04	0.16151E 07	0.36332E 04	0.45202E 01	0.44919E 01
0.10000E 01	0.26795E 00	0.26180E 00	-0.10845E 00	0.16937E 02	0.34927E-04	0.16973E 07	0.36105E 04	0.43819E 01	0.43575E 01

PLANE 7 ANGL =135.00 DEG
FIELD DATA
SHOCK ANGLES, DEG SIGMA= 17.5849 DELTA= -1.1334

X	R	THETA	PHI	P	RHO	H	V	M	M*
0.98792E 00	0.31302E 00	0.21284E 00	-0.12801E 00	0.22608E 02	0.47766E-04	0.16566E 07	0.36218E 04	0.44492E 01	0.44147E 01
0.98913E 00	0.30852E 00	0.21758E 00	-0.12421E 00	0.22765E 02	0.47737E-04	0.16691E 07	0.36183E 04	0.44283E 01	0.43958E 01
0.99034E 00	0.30401E 00	0.22229E 00	-0.12027E 00	0.22893E 02	0.47652E-04	0.16814E 07	0.36149E 04	0.44078E 01	0.43775E 01
0.99154E 00	0.29950E 00	0.22700E 00	-0.11617E 00	0.22995E 02	0.47512E-04	0.16939E 07	0.36114E 04	0.43874E 01	0.43592E 01
0.99275E 00	0.29499E 00	0.23172E 00	-0.11187E 00	0.23073E 02	0.47316E-04	0.17067E 07	0.36079E 04	0.43666E 01	0.43406E 01
0.99396E 00	0.29049E 00	0.23649E 00	-0.10735E 00	0.23129E 02	0.47062E-04	0.17201E 07	0.36042E 04	0.43451E 01	0.43214E 01
0.99517E 00	0.28598E 00	0.24132E 00	-0.10253E 00	0.23165E 02	0.46751E-04	0.17342E 07	0.36003E 04	0.43227E 01	0.43011E 01
0.99638E 00	0.28147E 00	0.24623E 00	-0.97272E-01	0.23179E 02	0.46387E-04	0.17489E 07	0.35962E 04	0.42996E 01	0.42803E 01
0.99758E 00	0.27696E 00	0.25126E 00	-0.91283E-01	0.23172E 02	0.45909E-04	0.17666E 07	0.35913E 04	0.42722E 01	0.42554E 01
0.99879E 00	0.27246E 00	0.25644E 00	-0.84510E-01	0.23144E 02	0.45049E-04	0.17981E 07	0.35825E 04	0.42242E 01	0.42103E 01
0.10000E 01	0.26795E 00	0.26180E 00	-0.77380E-01	0.23097E 02	0.43589E-04	0.18546E 07	0.35667E 04	0.41411E 01	0.41294E 01

PLANE 8 ANGL =157.50 DEG
FIELD DATA
SHOCK ANGLES, DEG SIGMA= 17.4726 DELTA= -0.6073

X	R	THETA	PHI	P	RHO	H	V	M	M*
0.98845E 00	0.31105E 00	0.20345E 00	-0.70028E-01	0.26303E 02	0.49165E-04	0.18725E 07	0.35617E 04	0.41154E 01	0.41059E 01
0.98960E 00	0.30674E 00	0.20951E 00	-0.67857E-01	0.26641E 02	0.49532E-04	0.18825E 07	0.35589E 04	0.41012E 01	0.40923E 01
0.99076E 00	0.30243E 00	0.21645E 00	-0.65606E-01	0.26935E 02	0.49837E-04	0.18916E 07	0.35563E 04	0.40884E 01	0.40801E 01
0.99191E 00	0.29812E 00	0.22131E 00	-0.63267E-01	0.27189E 02	0.50083E-04	0.19003E 07	0.35539E 04	0.40766E 01	0.40689E 01
0.99307E 00	0.29381E 00	0.22712E 00	-0.60827E-01	0.27404E 02	0.50272E-04	0.19079E 07	0.35517E 04	0.40656E 01	0.40585E 01
0.99422E 00	0.28950E 00	0.23290E 00	-0.58263E-01	0.27584E 02	0.50404E-04	0.19154E 07	0.35496E 04	0.40553E 01	0.40488E 01
0.99538E 00	0.28519E 00	0.23868E 00	-0.55527E-01	0.27728E 02	0.50474E-04	0.19227E 07	0.35475E 04	0.40452E 01	0.40394E 01
0.99653E 00	0.28088E 00	0.24445E 00	-0.52541E-01	0.27837E 02	0.50462E-04	0.19307E 07	0.35453E 04	0.40342E 01	0.40297E 01
0.99769E 00	0.27657E 00	0.25024E 00	-0.49196E-01	0.27912E 02	0.50334E-04	0.19409E 07	0.35424E 04	0.40204E 01	0.40158E 01
0.99884E 00	0.27226E 00	0.25601E 00	-0.45313E-01	0.27955E 02	0.50129E-04	0.19518E 07	0.35393E 04	0.40056E 01	0.40018E 01
0.10000E 01	0.26795E 00	0.26180E 00	-0.40884E-01	0.27959E 02	0.49963E-04	0.19586E 07	0.35374E 04	0.39965E 01	0.39934E 01

PLANE 9 ANGL =180.00 DEG
FIELD DATA
SHOCK ANGLES, DEG SIGMA= 17.4467 DELTA= 0.0000

X	R	THETA	PHI	P	RHO	H	V	M	M*
0.98854E 00	0.31070E 00	0.20019E 00	-0.58750E-09	0.27683E 02	0.49609E-04	0.19531E 07	0.35390E 04	0.40039E 01	0.40039E 01
0.98969E 00	0.30643E 00	0.20666E 00	-0.57174E-09	0.28087E 02	0.50114E-04	0.19617E 07	0.35365E 04	0.39924E 01	0.39924E 01
0.99083E 00	0.30215E 00	0.21300E 00	-0.55485E-09	0.28444E 02	0.50556E-04	0.19692E 07	0.35344E 04	0.39824E 01	0.39824E 01
0.99198E 00	0.29788E 00	0.21923E 00	-0.53696E-09	0.28756E 02	0.50940E-04	0.19758E 07	0.35325E 04	0.39737E 01	0.39737E 01
0.99313E 00	0.29360E 00	0.22538E 00	-0.51904E-09	0.29025E 02	0.51266E-04	0.19816E 07	0.35309E 04	0.39660E 01	0.39660E 01
0.99427E 00	0.28933E 00	0.23149E 00	-0.50234E-09	0.29252E 02	0.51535E-04	0.19867E 07	0.35295E 04	0.39593E 01	0.39593E 01
0.99542E 00	0.28505E 00	0.23756E 00	-0.48757E-09	0.29439E 02	0.51743E-04	0.19913E 07	0.35281E 04	0.39531E 01	0.39531E 01
0.99656E 00	0.28078E 00	0.24361E 00	-0.47286E-09	0.29587E 02	0.51886E-04	0.19958E 07	0.35269E 04	0.39473E 01	0.39473E 01
0.99771E 00	0.27650E 00	0.24967E 00	-0.45122E-09	0.29694E 02	0.51983E-04	0.19993E 07	0.35259E 04	0.39427E 01	0.39427E 01
0.99885E 00	0.27222E 00	0.25574E 00	-0.41598E-09	0.29762E 02	0.52100E-04	0.19994E 07	0.35259E 04	0.39426E 01	0.39426E 01
0.10000E 01	0.26795E 00	0.26180E 00	-0.37021E-09	0.29793E 02	0.52282E-04	0.19945E 07	0.35272E 04	0.39490E 01	0.39490E 01

THETA BODY =0.261799E 00